

## Research paper

# Architecture of shoreface to deep-water systems in segmented rift systems: Evidence from the southern margin of the Sogn Graben, northern North Sea

Xiaoan Zhong\*, Alejandro Escalona, Carita Augustsson

Department of Energy Resources, University of Stavanger, Norway

The spatial distribution of syn-rift deposits and temporal evolution of sandy gravity flows in the context of rift segmentation are poorly constrained. Based on conventional core description, well log analysis, and 3D seismic interpretation, this study focuses on the Upper Jurassic successions in the southern margin of the Sogn Graben, northern North Sea. Thirteen facies associations are classified in order to discuss the architecture of shoreface, gravity-driven submarine fans, and basin-plain deposits on the scale of centimeters to meters. In the eastern part of the study area, gamma-ray log stacking patterns suggest that northeast–southwest oriented shoreface successions underwent progradational-to-retrogradational deposition during the Oxfordian age. Lithological description of conventional cores indicates that large submarine fan system formed by debris-flow-dominated channels and turbidity-flow-dominated lobe complexes covers a broad (22 × 20 km) depositional area. The entry of regional drainages and the location of sandy gravity flow deposits were controlled by first-order rift segmentation, whereas the route of submarine canyon feeder system and the orientation of submarine fan lobes were determined by second-order rift segmentation. Thus, both first-order and second-order rift segmentation should be considered when determining the sedimentary facies and depositional architecture of sandy gravity flow deposits in individual rift segments.

## 1. Introduction

Conventional tectono-sedimentary models suggest that syn-rift tectonic activity plays significant role in controlling the location, sediment dispersal patterns, and channel development of submarine fans (Prosser, 1993; Ravnås and Steel, 1998; Gawthorpe and Leeder, 2000). For example, the orientation and movement of rift-border faults have an impact on the depositional processes and stacking patterns of submarine fans throughout the cycle of non-segmented rift systems (Ravnås and Bondevik, 1997; Wells, 1999). Previous studies have suggested that reactivation of rift fabric is capable of offsetting graben axes (McClay et al., 2002; Fossen et al., 2010) and resulting in along-axis segmentation (Hayward and Ebinger, 1996; Ebinger et al., 1999; Rowland and Sibson, 2004; Ebinger, 2005; Corti, 2008). Rift segmentation has significant implications for the evolution of border-fault systems and, therefore, determines the variability of the syn-rift stratigraphy differently to non-segmented systems (Upcott et al., 1996; Khalil and McClay, 2001; Rowland and Sibson, 2001; Wolfenden et al., 2004; Zhong et al., 2018). Previous studies have mainly focused on the mechanism and evolution of segmented rift systems at basin scale and little work has documented the sedimentary record within individual segments (Hayward and Ebinger, 1996; Upcott et al., 1996; Rowland and Sibson, 2001; Wright et al., 2006; Corti, 2008). Thus, the detailed

temporal evolution of gravity flows and spatial distribution of related syn-rift deposits in the context of rift segmentation remain poorly constrained.

Zhong and Escalona (in press) proposed that the Jurassic rift system in the northern North Sea was a product of rift segmentation, which was initiated by oblique extension during the Middle Jurassic–Early Cretaceous (Fig. 1). The north-trending Jurassic rift system was segmented in a multi-order motif by twofold structural elements: (1) the EN–E–WSW-striking Horda–Uer and Ryggsteinen–Sogn fault transfer zones that were created by the synthetic shear component along pre-existing Caledonian-age (Silurian–Devonian) structures (cf. Fazlikhani et al., 2017; Fossen et al., 2017). They resulted in the first-order rift segmentation and divided the northern North Sea into three segments (C1, C2, and C3; Fig. 1a); and (2) the NNW–SSE-striking oblique-slip faults that were created by the antithetic shear component. They induced the second-order rift segmentation and caused internal deformation within individual rift segments (Fig. 1).

This study reveals the distribution, architecture, and sedimentary processes of Upper Jurassic shoreface to deep-water deposits in the southern margin of the Sogn Graben, northern North Sea, by linking conventional core descriptions, well-log, and seismic interpretation. The goal is to develop a predictive model for internal architecture, spatial distribution, and the character of subaqueous sandy gravity

\* Corresponding author.

E-mail address: [xiaoan.zhong@hotmail.com](mailto:xiaoan.zhong@hotmail.com) (X. Zhong).

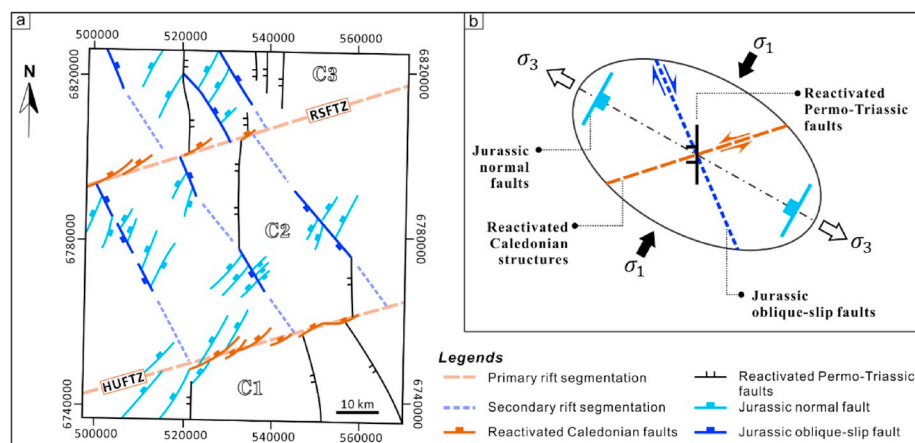


**Fig. 1.** Conceptual model of multi-order rift segmentation in the northern North Sea. Note that two major fault transfer zones primarily divided the Jurassic rift system into three segments (C1, C2, and C3). Individual rift segments were secondarily segmented by Jurassic oblique-slip faults. (a) The distribution of simplified fault segments and proposed rift segmentations; (b) The Jurassic oblique-rifting strain field and associated fault populations. Modified after Zhong and Escalona (in press). Abbreviations: HUFTZ, Horda-Uer Fault Transfer Zone; RSFTZ, Ryggsteinen-Sogn Fault Transfer Zone.

flows (*sensu* Marr et al., 2001) as a function of rift segmentation by characterizing the sedimentary variability of the Upper Jurassic syn-rift successions.

## 2. Geological setting

The structural evolution of the northern North Sea includes Permo-Triassic and Jurassic rifting stages, which resulted in sequential faulting and interference between N-S- and NE-SW-striking faults (Nottvedt et al., 1995; Færseth et al., 1997; Odinsen et al., 2000b). Four fault populations that are related to Late Jurassic rifting have been proposed (Fig. 1): (1) the reactivated Caledonian ENE-WSW-striking normal faults (Fazlikhani et al., 2017; Fossen et al., 2017); (2) north-south-striking normal faults that were inherited from the Permo-Triassic rifting (Bartholomew et al., 1993; Odinsen et al., 2000a); (3) north-east-south-west-striking normal faults that were created by the Jurassic rifting (Færseth et al., 1997; Whipp et al., 2014); and (4) the NNW-SSE-striking oblique faults that are also related to the Jurassic rifting (Zhong and Escalona (in press)).

In the northern North Sea, the Sogn Graben is flanked by the Marflo Spur to the west and the Måløy Slope to the east (Fig. 2). The crystalline basement was interpreted about 9 km below the seabed in the Sogn Graben depocenter (Hospers and Ediriweera, 1991). A major structural high, the Ryggsteinen Ridge, was developed at the southern margin, where several hydrocarbon-bearing Upper Jurassic reservoirs have been discovered since the 1970s (NPD, 2019).

The Upper Jurassic interval of this study covers the Oxfordian, Kimmeridgian, and Tithonian stages (Zeiss, 2003). Upper Jurassic successions are included in the Viking Group (Fig. 3), in which some wells contain the Fensfjord Formation and all contain the Heather, Sognefjord, and Draupne formations (Vollset and Doré, 1984). In the northern North Sea, the Heather and Draupne formations are dominated by marine shale, which serves as an important source rock for Upper Jurassic petroleum systems (Gormly et al., 1994). In the Oseberg-Brage area, 20 km southwest of the study area, the Fensfjord and Sognefjord formations contain fine-grained sandstones of low-density turbidites (Ravnås and Bondevik, 1997). At the Horda Platform, 3 km south of the study area, the Fensfjord and Sognefjord formations were deposited in shallow-marine to shoreface environments (Stewart et al., 1995), indicating a large variability of deposition systems.

In the southern Sogn Graben, the thickness of the preserved Upper Jurassic strata drastically changes from one rift segment to another (Fig. 4). The strata in the hanging-walls of major normal faults present prominent wedge-shaped (Fig. 4b) or tabular (Fig. 4d) geometries, which are related to the combination of syn-rift differential loading and fault-block rotation (Crans et al., 1980; Nottvedt et al., 1995; Ravnås and Bondevik, 1997).

## 3. Data and methods

This study focuses on a 4250 km<sup>2</sup> area offshore Norway (Fig. 2). A 3D seismic dataset, merged from cubes with 25 m bins by PGS Reservoirs Ltd., covers the whole study area. Since the 1980s, 52 exploration and appraisal wells have been drilled and acquired with well datasets including wireline logs, check shots, conventional cores, and cuttings. For the purpose of correlating Upper Jurassic stage-by-stage intervals, the depositional sequence boundaries were picked by internal biostratigraphic analysis done by Ichron and Geolink. The sequential framework sub-divides the Oxfordian, Kimmeridgian, and Tithonian into nine (Ox0-Ox8), seven (Ki1-Ki7), and six (Ti1-Ti6) third-order sequences (or sub-stages), respectively (cf. Jacquin et al., 1998). The synthetic seismogram of well 35/12-5S shows a satisfactory tie between time and depth domains (Fig. 3). Structural maps were generated along the tops of the Callovian, Oxfordian, Kimmeridgian, and Tithonian seismic sequences. Thickness maps for the Oxfordian, Kimmeridgian, and Tithonian were produced to show the distribution of preserved strata. Conventional cores from exploration wells show that Upper Jurassic deposits in the study area are dominated by conglomerate, sandstone, siltstone, and claystone (grain size after Wentworth, 1922). In order to classify the facies of the Upper Jurassic deposits, conventional cores from wells 36/7-1, 35/35/9-7, 35/11-11, and 35/11-6 are described lithologically. Classification of facies associations is based on sedimentological characteristics, lithological patterns, microfossils, and flow processes as described by Bouma (1962), Ravnås and Bondevik (1997), Hodgson (2009), Kernén et al. (2012), among others. Flow processes that led to shoreface to deep-water deposition are inferred from sedimentary structures in the cores. Facies associations are interpreted for the entire Upper Jurassic interval by (1) linking millimeter-scale architecture from conventional core descriptions to well-log responses, (2) correlating time-equivalent intervals in neighboring cores, and (3) complementing with seismic amplitude continuities. The Upper Jurassic clastic rocks are classified into three first-order facies associations under the framework of shoreface to deep-water systems (Table 1). The shoreface facies associations record gradual basinward variations in lithology and architecture, whereas the submarine-fan facies associations are laterally expressed by channel, lobe, and fringe. This provides a predictive model along axial inner-middle-outer fan direction.

## 4. Facies associations

### 4.1. Shoreface (Facies association I)

Facies Association I includes a stratigraphic transition from cross-stratified coarse-grained sandstone, cross-stratified medium-grained

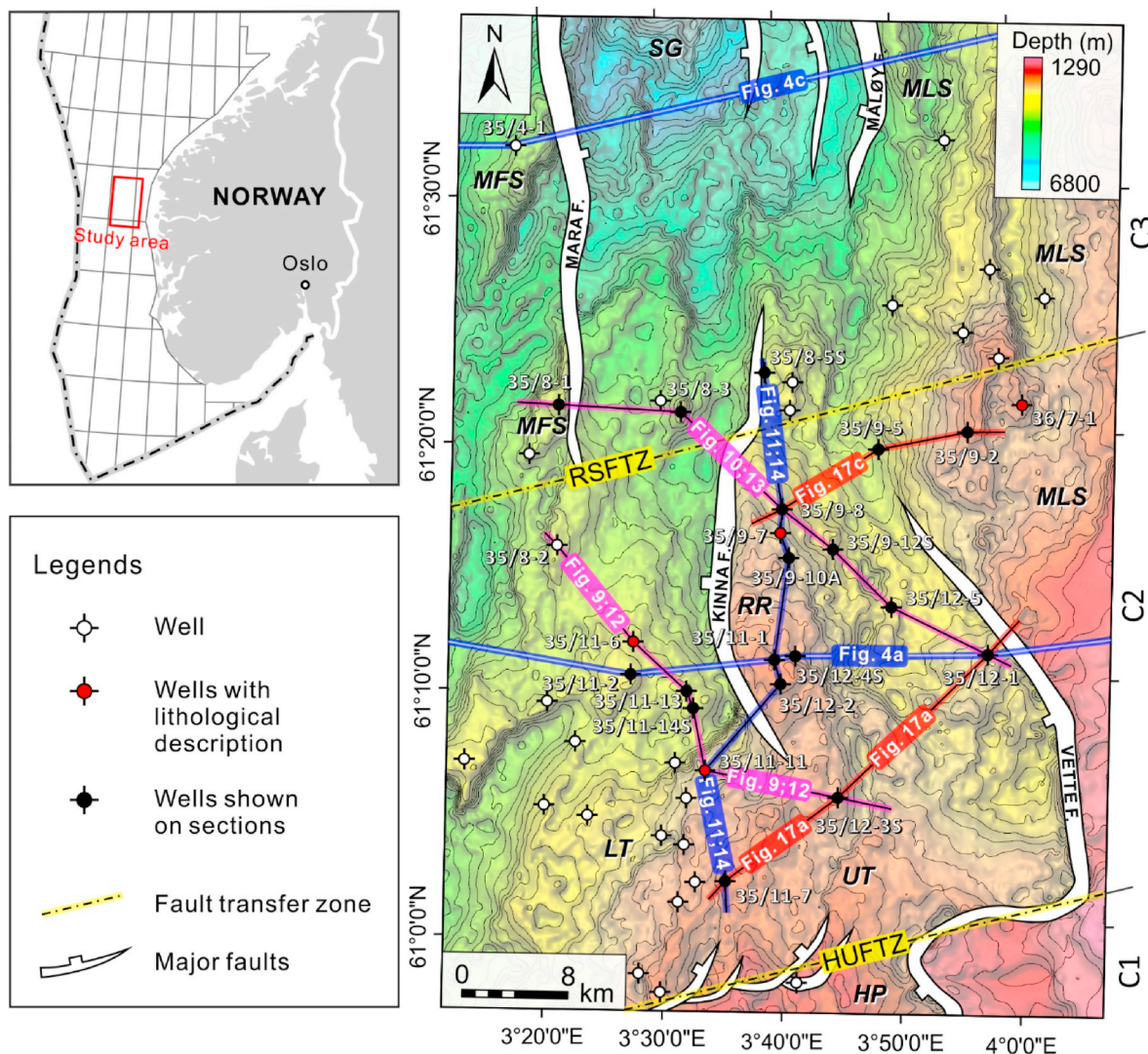


Fig. 2. Location map of the study area in offshore Norway. The base grid is the two-way-time depth map of the Base Cretaceous Unconformity. Note that C1, C2, and C3 are major segments as the result of rift segmentation. Abbreviations: HP, Horda Platform; HUFTZ, Horda–Uer Fault Transfer Zone; LT, Lomre Terrace; MFS, Marfloy Spur; MLS, Måløy Slope; RR, Ryggsteinen Ridge; RSFTZ, Ryggsteinen–Sogn Fault Transfer Zone; SG, Sogn Graben; UT, Uer Terrace.

sandstone, to bioturbated or hummocky laminated fine-grained sandstone. Accordingly, 3 s-order facies associations are identified from top to bottom (Table 1):

- (1) Facies Association I-1 is represented by overall upward-decreasing gamma-ray values from moderate (70–90 API) to low (< 70 API). This facies association comprises decimeter-to meter-scale beds of moderately sorted, medium-to coarse-grained, quartz-rich sandstones (Table 1; Fig. 5a, b, and e). Cross-stratification is defined by silty drapes. Sparse bioturbation with burrows are found. Shell fragments of mixed assemblage are locally observed (Fig. 5e).
- (2) Facies Association I-2 is represented by stacked gamma-ray intervals of overall upward-decreasing values in a moderate range (70–90 API; Table 1). This facies association consists of well-to locally poorly sorted, medium-grained, slightly silty sandstone beds (Table 1; Fig. 5a). Decimeter-scale sandstone layers display ripple to medium-scale (0.3–6 m in length, sensu Mckee and Weir, 1953) cross-stratification and diffuse mottled fabric towards the top (Fig. 5d). Bioturbation (mostly *Diplocraterion*, *Ophiomorpha*, and

*Paleophycus*) is sporadic.

- (3) Facies Association I-3 is represented by high gamma-ray values (90–150 API) with occasional peaks of moderate values (Table 1). These peaks show overall upward-decreasing values. This facies association includes well sorted, fine-grained, slightly silty sandstone. Centimeter-to decimeter-scale beds include swaley or hummocky cross-stratification. Sandy beds are weakly to moderately bioturbated by burrows, escape traces, etc. *Chondrites* and *Schaubcylindrichnus* are observed (Fig. 5c).

#### 4.1.1. Interpretation

The presence of *Chondrites* and *Phycosiphon* trace fossils was common in Upper Jurassic highly bioturbated, storm-influenced shoreface deposits in the southern North Sea (cf. Baniak et al., 2014). The lithological variations and different types of cross stratifications in the study area point to a deposition in shoreface environment (cf. Hampson and Storms, 2003). Therefore, 3 s-order facies associations I-1, I-2, and I-3 are interpreted as upper, middle, and lower shoreface, respectively. The key of differentiating Facies Associations I-3 (Lower

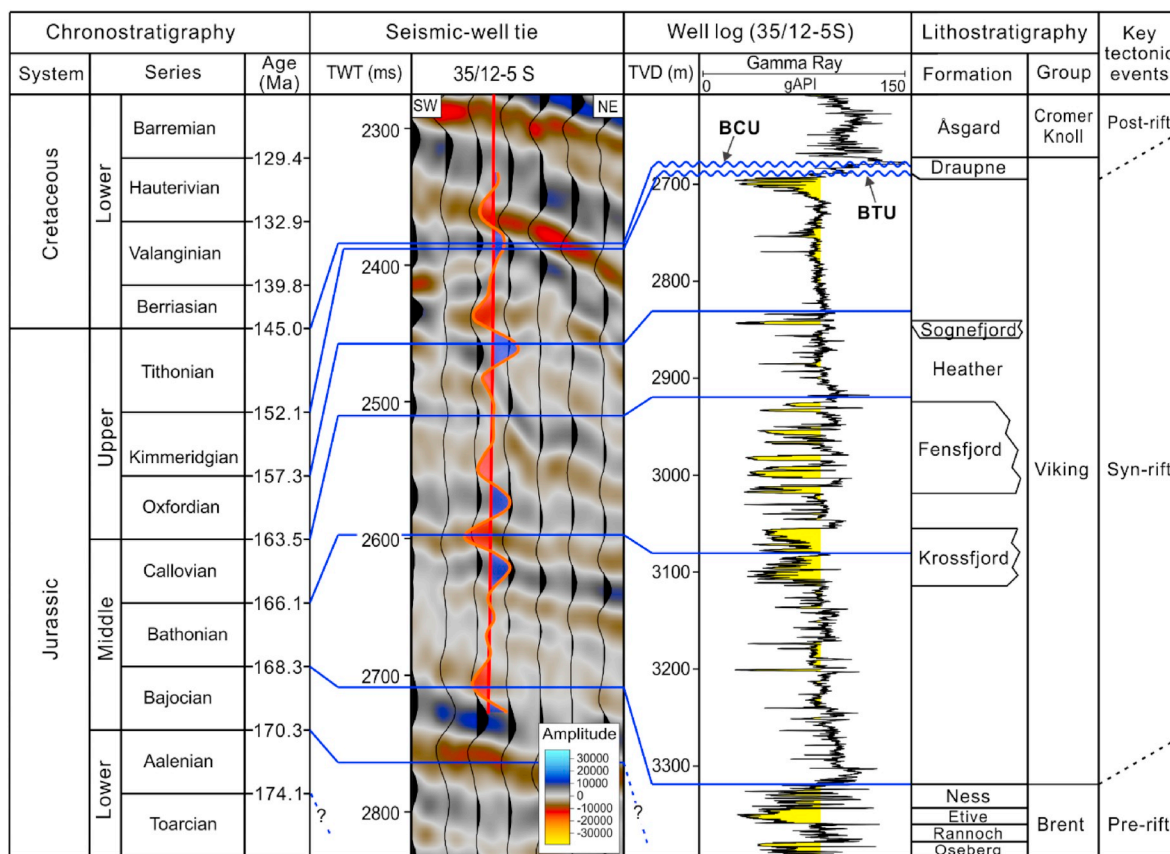


**Fig. 3.** Regional-stratigraphic framework of the northern North Sea. Seismic data is Reverse Polarity (SEG Convention), whereby a trough (red) represents an increase in acoustic impedance and a peak (blue) a decrease in acoustic impedance. Key tectonic events are after Ravnås et al. (2000). Abbreviations: TWT, two-way-time; TVD, total vertical depth; BCU, Base Cretaceous unconformity; BTU, Base Tithonian unconformity. (For interpretation of the references to colour in this figure legend, the reader is referred to the Web version of this article.)

shoreface) from Facies Associations I-1 (Upper shoreface) is outboard-fining grain sizes, decreasing sandstone bed thickness, swaley or hummocky cross-stratification, and increasing bioturbation and claystone content.

#### 4.2. Submarine fans (Facies association II)

Facies Association II includes a lithological transition from inverted- or normal-graded conglomerate, via massive or normal-graded coarse sandstone, to normal-graded medium or fine sandstone. Three second-order facies associations are categorized, from proximal to distal, II-1, II-2, and II-3 (Table 1).

(1) Facies Association II-1 is dominated by meter-to decimeter-scale beds of pebbly conglomerate or coarse-grained sandstone. Shell fragments are locally observed at the base. In the central part, conglomeratic or coarse sandstone beds have sharp bases. They are thinning towards the west, coupled with a gradual decrease in grain size. Therefore, they are classified into the architectural elements channel, lobe, and fringe that form three third-order facies associations: (a) Facies Association II-1a is featured by varying gamma-ray values from moderate, via low, to moderate (Table 1). This facies association consists of meter-scale amalgamated beds of clast-supported pebbly conglomerate with erosive bases, grading into moderately to well sorted, pebbly, medium-grained sandstones (Fig. 6a and c). The conglomerate matrix corresponds to moderately sorted, medium-to coarse-grained sandstone. Inversely graded clasts at the base are sub-horizontally aligned pebbles and cobbles of laminated claystone and cemented sandstones (Fig. 6c). (b)

Facies Association II-1b has overall upward-increasing gamma-ray values from low to moderate (Table 1). This facies association comprises decimeter-scale beds of moderately to well sorted, medium-grained to pebbly sandstones (Fig. 6a and b). The sandstones are structureless or display normal-graded planar lamination. Abundant claystone and cemented sandstone clasts are notable in the lower part of beds. (c) Facies Association II-1c has overall upward-increasing gamma-ray values in the moderate range (Table 1). This facies association contains decimeter-scale beds of moderately sorted, medium-to coarse-grained structureless sandstone. Sub-rounded to rounded claystone clasts are notable. Compared to Facies Association II-1b, the individual beds are much thinner. Sandstone beds that rest directly on dark-grey silty claystone have erosive bases.

(2) Facies Association II-2 is dominated by amalgamated decimeter-scale beds of coarse-to medium-grained sandstones (Table 1). Similar to Facies Association II-1, three third-order facies associations are classified: (a) Facies Association II-2a is featured by low gamma-ray values with an upward-decreasing trend at the base and an upward-increasing trend at the top (Table 1). This facies association is composed of amalgamated decimeter-scale beds of pebbly, moderately to locally well sorted, coarse-grained sandstones mixed with common claystone clasts (Fig. 7a and e). Occasional pyrite enrichment, shell and belemnite fragments occur. (b) Facies Association II-2b has overall upward-increasing gamma-ray values in the low range (Table 1). It comprises amalgamated decimeter-scale beds of variably poorly to well sorted, coarse-grained sandstones that mostly are fining upwards and contains quartz pebbles, granules and very coarse sand grains that are concentrated

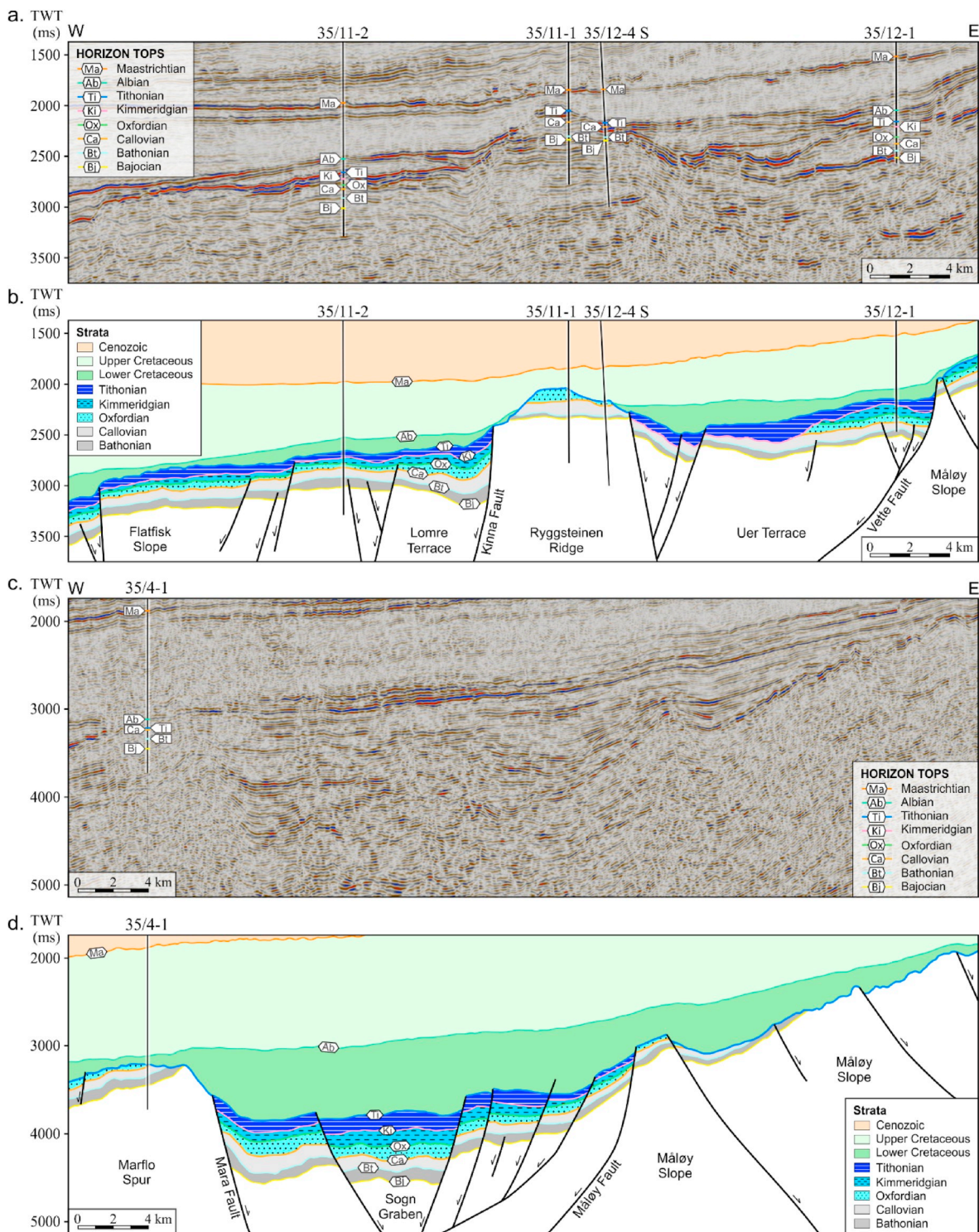


Fig. 4. Seismic lines showing structural elements, faults, and stratigraphic patterns. (a) Original seismic profile through rift segment C2; (b) Interpreted seismic profile through rift segment C2; (c) Original seismic profile through rift segment C3; (d) Interpreted seismic profile through rift segment C3. Their geographical positions are given in Fig. 2. Abbreviations: Bj, Bajocian; Bt, Bathonian; Ca, Callovian; Ox, Oxfordian; Ki, Kimmeridgian; Ti, Tithonian; Ab, Albian; Ma, Maastrichtian.

in basal lags (Table 1; Fig. 7d; Fig. 8b). The concentration of pyrite is common. The beds are normally structureless but locally they display grain-size stratification (Fig. 7d; Fig. 8c). (c) Facies Association II-2c has overall upward-increasing gamma-ray values in the moderate range (Table 1). It consists of amalgamated decimeter-scale beds of moderately to well sorted, medium-grained sandstones that are fining upwards. Coarse sandstone grains are found in structureless basal lags. Occasional dewatering structures are

present. Planar stratification is highlighted by organic-rich laminae at the top of the beds.

(3) Facies Association II-3 is dominated by centimeter-scale beds of fine-to very-fine-grained sandstones interbedded with thin claystone layers (Table 1). Individual beds usually display a rhythmic sequence that begins with irregular basal laminae of fine-grained sandstones followed by regular parallel silty laminae and ends with ungraded claystone (Fig. 8d). Similar to facies associations II-1 and

II-2, three third-order facies associations are classified: (a) Facies Association II-3a is featured by stacking intervals of moderate to low gamma-ray values (Table 1). Each interval has upward-increasing values. The facies association consists of centimeter-thick beds of moderately to well sorted, fine-grained sandstones intercalated with dark-grey laminated siltstone layers. The sandstone beds are fining upwards and structureless to locally laminated (< 2 cm) with frequent up to 1 cm long claystone clasts. Medium-grained tractional lags are present at the sandy bases. The trace fossils *Chondrites* and *Phycosiphon* occur sporadically. (b) Facies Association II-3b is featured by isolated intervals of upward-increasing gamma-ray values in the moderate range (Table 1). It comprises planar laminated siltstone and claystone with subordinate well sorted, very-fine-grained, sandstones (Fig. 8d). Siltstone and claystone layers display frequent sandy pinstripes. Centimeter-scale sandstone beds are locally ripple-laminated and display fining upwards heteroliths. No erosion or tractional lags are observed at the base of the sandstone beds. (c) Facies Association II-3c is characterized by spikes of moderate gamma-ray values standing tall and upright on the high gamma-ray interval. The high values correspond to dark grey to black, planar laminated claystone (Table 1). The spikes correspond to very fine-grained, millimeter-to centimeter-scale sandstone pinstripes that occasionally display ripple-scale cross-lamination.

#### 4.2.1. Interpretation

Sporadic *Chondrites* and *Phycosiphon* trace fossils in sediments support mostly anoxic conditions (cf. Bromley and Ekdale, 1984). Facies Association II is interpreted as deep-water submarine fans driven by sandy gravity flows (cf.; Ghibaudo, 1992; Stow and Johansson, 2000; Mulder and Alexander, 2001; Talling et al., 2012). The inverted grading, tractional lags, and erosive bases of the conglomeratic infills in Facies Association II-1 point to the inner fan, which is dominated by debris flows (cf. Middleton and Hampton, 1973; Ghibaudo, 1992). The clast- and matrix-supported conglomerate beds indicate transport of cohesionless and cohesive debris flows, respectively (cf. Mulder and Alexander, 2001). The lithological characters of normal-graded sandy units in facies associations II-2 and II-3 are interpreted as middle and outer fan, respectively, with a dominance of turbidity-flow deposition (cf. Bouma, 1962; Postma and Cartigny, 2014). Third-order channel-lobe-fringe facies associations indicate architecture variations along the dip of submarine fans (cf. Picot et al., 2016; Hofstra et al., 2017; Bell et al., 2018). Enrichment of pyrite suggests deposition under euxinic conditions (cf. Raiswell and Berner, 1985).

#### 4.3. Offshore claystone in basin plain (Facies association III)

Facies Association III is represented by high to extremely high (> 150 API) gamma-ray values (Table 1). The lithology is dominated by millimeter-laminated, dark-grey, silty claystone that in places is highly bioturbated with *Chondrites*, *Phycosiphon*, and *Schaubcylichnus* (Fig. 6d). Belemnites are occasionally found (as arrowed in Table 1).

#### 4.3.1. Interpretation

The dark-grey claystone is interpreted as offshore marine deposits (cf. Vollset and Doré, 1984). Thus, Facies Association III points to a basin-plain environment (cf. Ravnås et al., 2000).

### 5. Upper Jurassic sequences and sedimentary architectures

Upper Jurassic successions include the Oxfordian, Kimmeridgian, and Tithonian sequences (Fig. 3). The exploration wells show that the thickness of preserved Upper Jurassic sequences varies drastically in the

study area (Fig. 9 to Fig. 11). The Oxfordian stage is usually thicker than the Kimmeridgian and Tithonian stages.

#### 5.1. Oxfordian

##### 5.1.1. Well correlations

The Oxfordian stage is incompletely preserved, often lacking the top (Figs. 9–11). Occasional absence of sub-stages at the base is observed from wells 35/9-10A and 35/9-7 (Fig. 11). Low gamma-ray responses indicate that the middle Oxfordian (sub-stages Ox3–5) contains more sandstones than the lower (sub-stages Ox0–2) and upper (sub-stages Ox6–8) parts.

In the southern part of the study area, the thickness of the Oxfordian stage normally decreases from east to west, which for example can be seen in wells 35/12-3S (268 m), 35/11–13 (248 m), and 35/11-6 (173 m; Fig. 9). In the middle part of the study area, a similar east–west or southeast–northwest migration trend is observed for bulk sandstones or conglomerates through sub-stages along wells 35/9-12S, 35/9-8, and 35/8-3. Well 35/12-5S in the east lacks gross sandstones (Fig. 10). Similarly, intervals with mostly sandstones shift stratigraphically from well 35/11–13 in the center of the study area (sub-stages Ox2–5), via well 35/11-6 (sub-stages Ox4–5), to well 35/8-2 (sub-stages Ox4–6) in the west.

The sandy packages in all wells but 35/12-3S are from Facies Association II (Fig. 9). Well 35/12-3S in the southeast comprises multiple upward-coarsening sandstone packages from Facies Association I. Thus, a major facies change appears within a distance of 10 km to the closest well further northwest (35/11-11; Fig. 9). Well 35/11-6 in the northwest records alternations of Facies Association II-3 and adjacent Facies Association II-2 in well 35/11–13. The northwest-directed sedimentary facies changes also can be seen from Facies Association I (shoreface in well 35/12-1), via Facies Association II-1 (inner fan in wells 35/12-5S and 35/9-12S) and Facies Association II-2 (middle fan in well 35/9-8), to Facies Association II-3 (outer fan in wells 35/8-3 and 35/8-1), and eventually ended up with Facies Association III within a 30-km distance from southeast to northwest (Fig. 10). Similarly, in the northern part of the Ryggsteinen Ridge, middle Oxfordian (sub-stages Ox3–5) sedimentary facies show a transition from Facies Association II-1 (inner fan) in wells 35/9-10A and 35/9-7 in the center of the study area, via Facies Association II-2 (middle fan) in well 35/9-8, to Facies Association II-3 (outer fan) and Facies Association III (offshore claystone) in well 35/8-5S (Fig. 11). In general, submarine fan system is SE–NW orientated showing that wells in the southeast (e.g. wells 35/11-1, 35/11-7, 35/12-2, and 35/12-3S) are dominated by Facies Association I (shoreface), wells in the middle (e.g. 35/11-11, 35/11–13, 35/11-14S, 35/9-7, 35/9-10A) are dominated by facies associations II-1 (inner fan) and II-2 (middle fan), and wells in the west and northwest (e.g. 35/11-6, 35/8-2, 35/8-1, 35/8-3, 35/8-5S) are dominated by Facies Association II-3 (outer fan; Figs. 9–11).

##### 5.1.2. Seismic data

The Oxfordian seismic sequence is usually unconformably overlain by younger sequences in the Uer Terrace, the Lomre Terrace, the Ryggsteinen Ridge, and the Marflo Spur (Fig. 12 to Fig. 14). At the Uer Terrace in the southeast, the Oxfordian is lacking as seismic reflectors of the Middle Jurassic Bathonian and Callovian sequences are truncated by a continuous reflector along the base of the Kimmeridgian (between wells 35/11-11 and 35/12-3S; Fig. 12). In the eastern part of the Ryggsteinen Ridge, seismic reflectors of the Callovian, Oxfordian, and Kimmeridgian are truncated by the base-Tithonian horizon, forming two notches on top of the Oxfordian sequence in the area of wells 35/9-12S, 35/12-5S, and 35/12-1 in the east (Fig. 13). Similar notches are present in the northern part of the Ryggsteinen Ridge (Fig. 14).

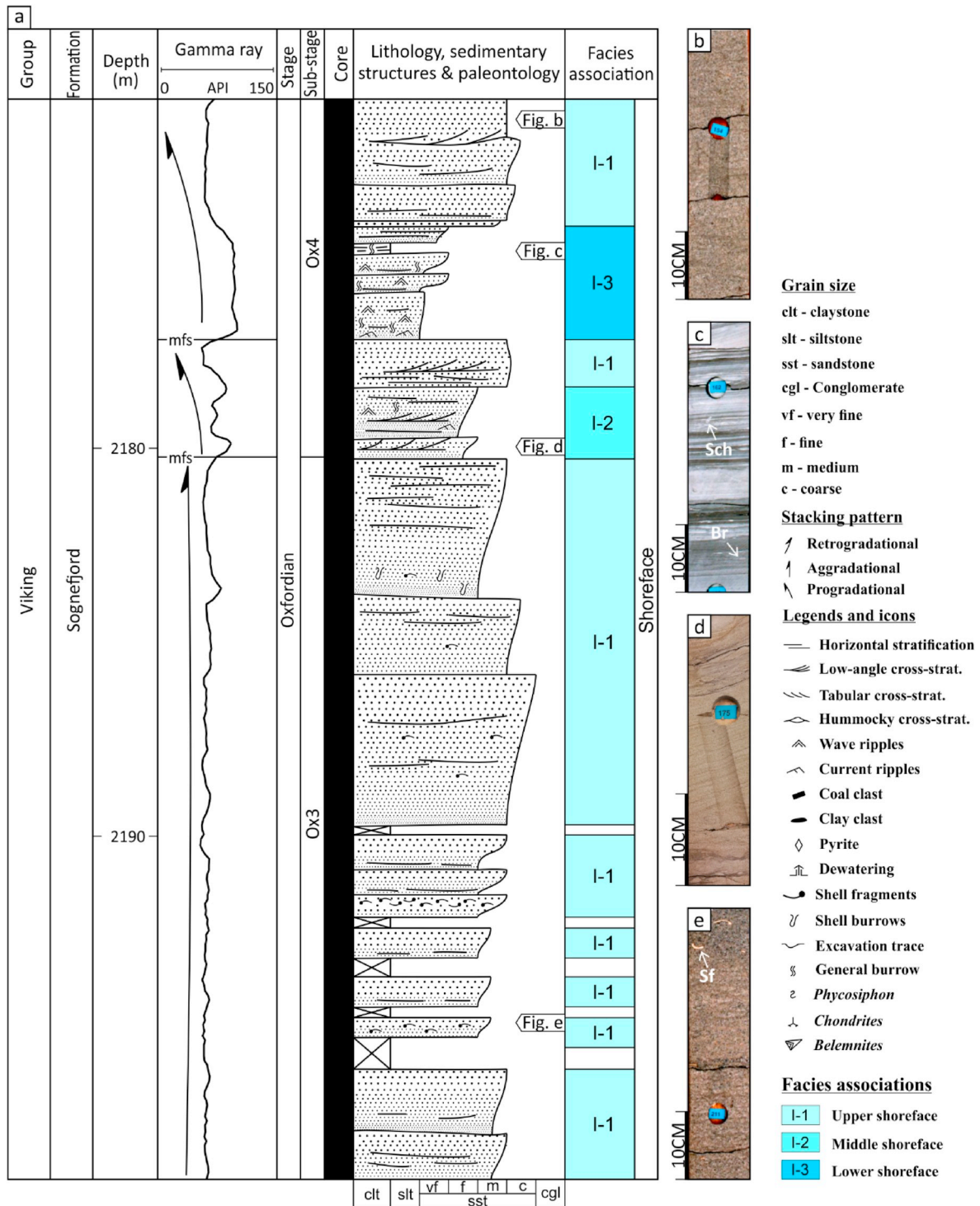


Fig. 5. Sedimentological logs of well 36/7-1 with shoreface facies associations. Well location in Fig. 2. Abbreviations: Br, burrows; Sch, *Schaubicylindrichnus*; Sf, shell fragment; F. A., facies association; mfs, marine flooding surface.

5.1.3. Structural and thickness maps

The Oxfordian stage is mainly missing in the footwall of the Kinna Fault and on the Måløy Slope near the Vette Fault (Fig. 16a). The top Oxfordian shows a gradual topographic descent from the southeast to the northwest, composed of stepped structures from south to north and east to west (from segment C1 and the Måløy Slope to segment C3 and the Marflo Spur; Fig. 15a). The south-to-north stepping is separated by the Horda-Uer and Ryggsteinen-Sogn fault transfer zones (*sensu*, Zhong and Escalona (in press)).

5.1.4. Interpretation

The Base Oxfordian Unconformity (Fig. 11; Fig. 14) and the Base Kimmeridgian Unconformity (Figs. 9–14) are proposed as names for the unconformities along discontinuous Callovian–Oxfordian and Oxfordian–Kimmeridgian contacts. The Base Oxfordian and Base Kimmeridgian unconformities are mostly present on both footwall areas of tilted fault blocks as well as horst blocks. Therefore, they are interpreted to represent periods of submarine erosion above fair weather wave base as well as subaerial exposure during Oxfordian time. The

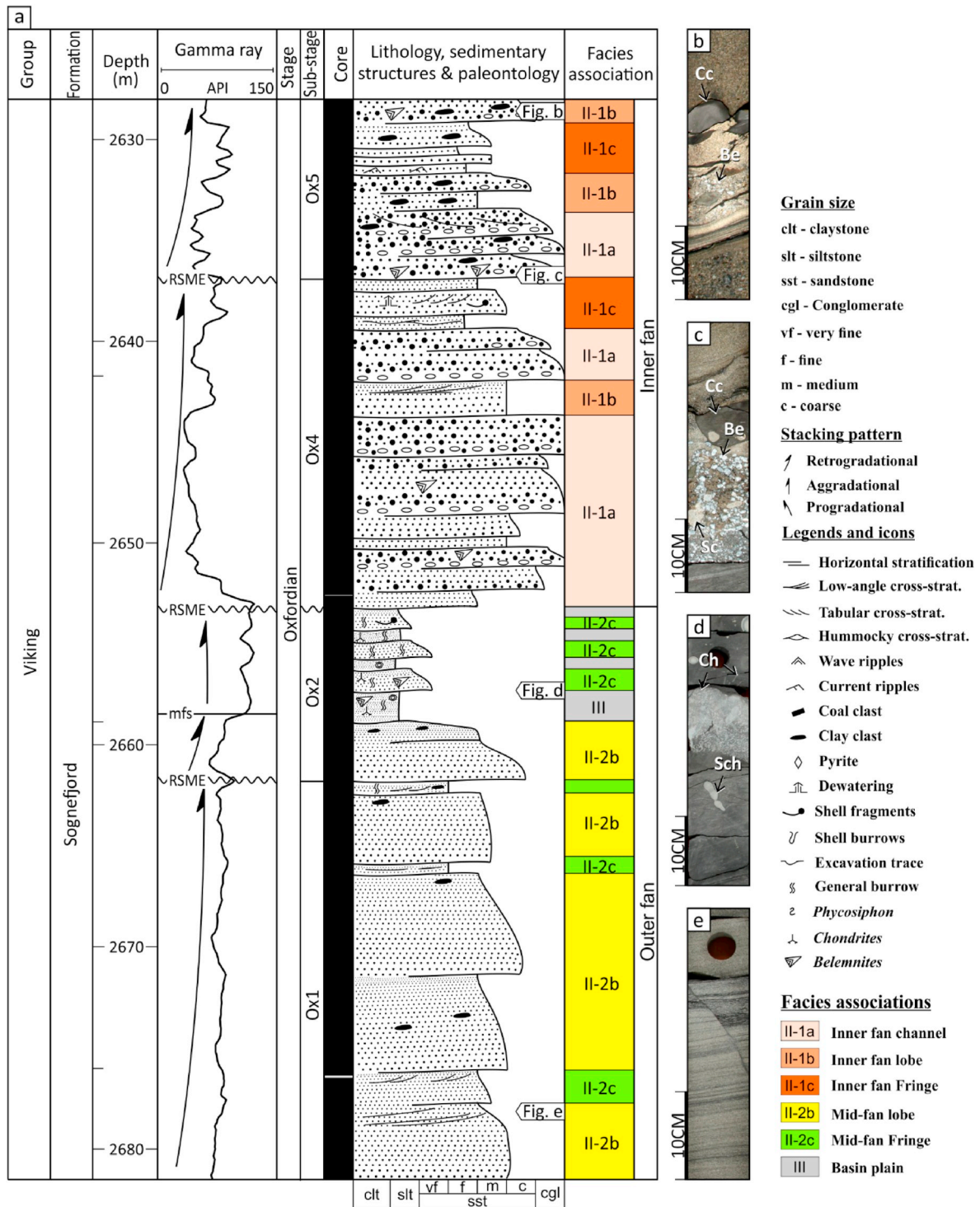


Fig. 6. Sedimentological logs of well 35/9-7 showing submarine mixed middle-inner fan facies associations. Well location in Fig. 2. Abbreviations: Be, belemnite; Cc, claystone clast; Ch, Chondrites; Sc, sand clast; Sch, Schaubcylichnus; F. A., facies association; mfs, marine flooding surface; RSME, regressive surface of marine erosion.

notches on top of the Oxfordian may have been resulted from antithetic normal faulting or erosion. Seismic truncation from the base (Fig. 12) and prominent absence/thinning of Oxfordian suggest probably incisional processes. As such, these notches are interpreted to be the incision of submarine channels, forming an important part of the Base

Kimmeridgian Unconformity. Gamma-ray patterns with an upward-coarsening trend in Facies Association I is interpreted as the result of upward-shallowing and progradational shorelines (cf. Ravnås et al., 1997). This barely affects Facies Association II (Submarine fan) in the middle and western part, where Gamma-ray logs show prominent

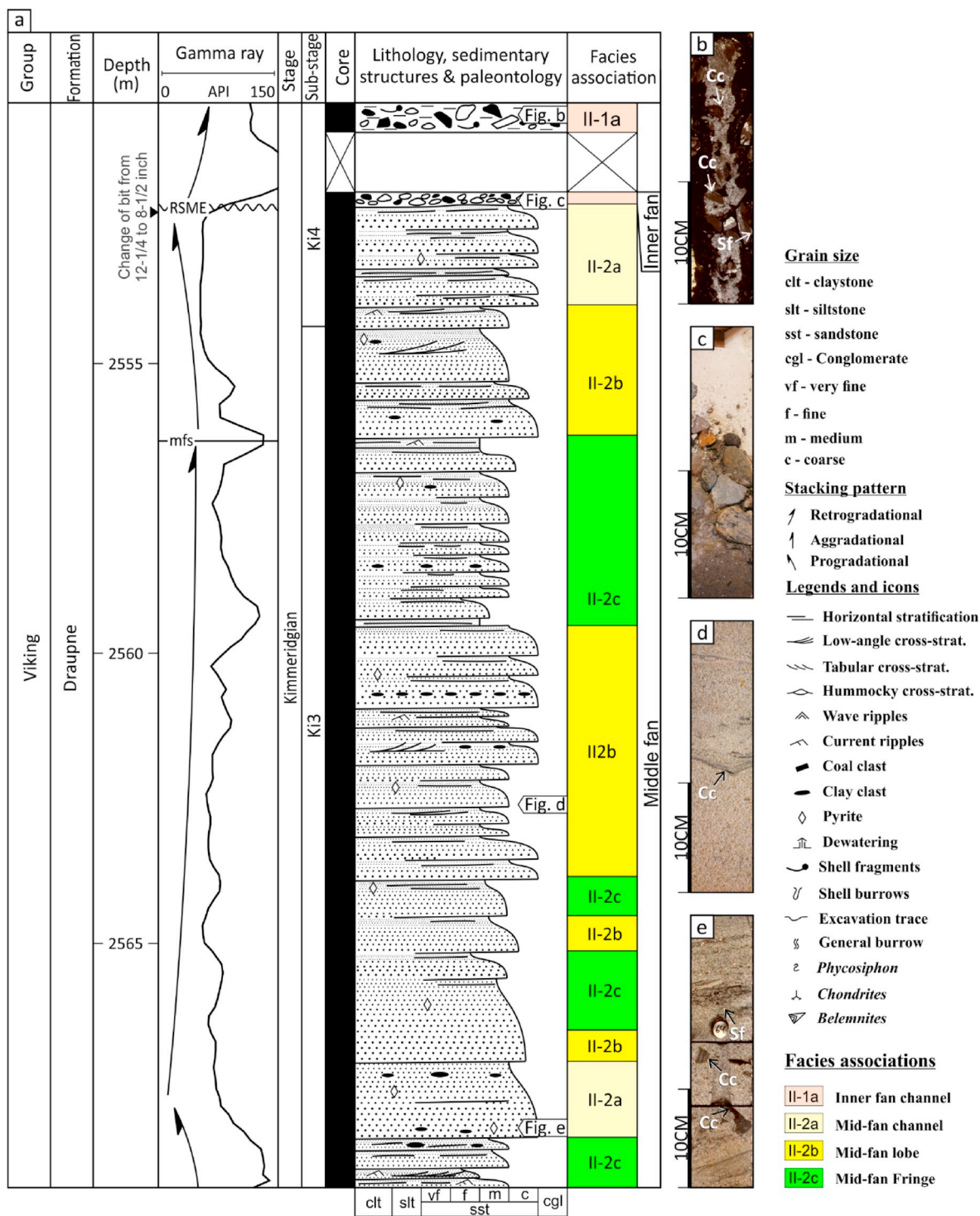


Fig. 7. Sedimentological logs of well 35/11-11 showing submarine middle fan facies associations. Well location in Fig. 2. Abbreviations: Cc, claystone clast; Sf, shell fragment; F. A., facies association; mfs, marine flooding surface; RSME, regressive surface of marine erosion.

upward-fining trends (Fig. 9; Fig. 10). The east-to-west facies trend indicates that sediments were derived from the east. Particularly for the middle Oxfordian, a progradational depositional system is interpreted based on (1) high sandstone content in the middle Oxfordian (sub-stages Ox3–5), (2) westward-migrated bulk sandstone unit through sub-stages, and (3) a northwest-directed migration of second-order facies

associations (Figs. 9 and 10). The depositional system retrograded during the late Oxfordian based on decreased sandstone beds and vertical facies association transition towards a more distal environment. The progradational to retrogradational evolution of depositional systems is interpreted as an increase in accommodation space, which can be caused by flexural downbending in the hanging-wall blocks (cf. Hoth

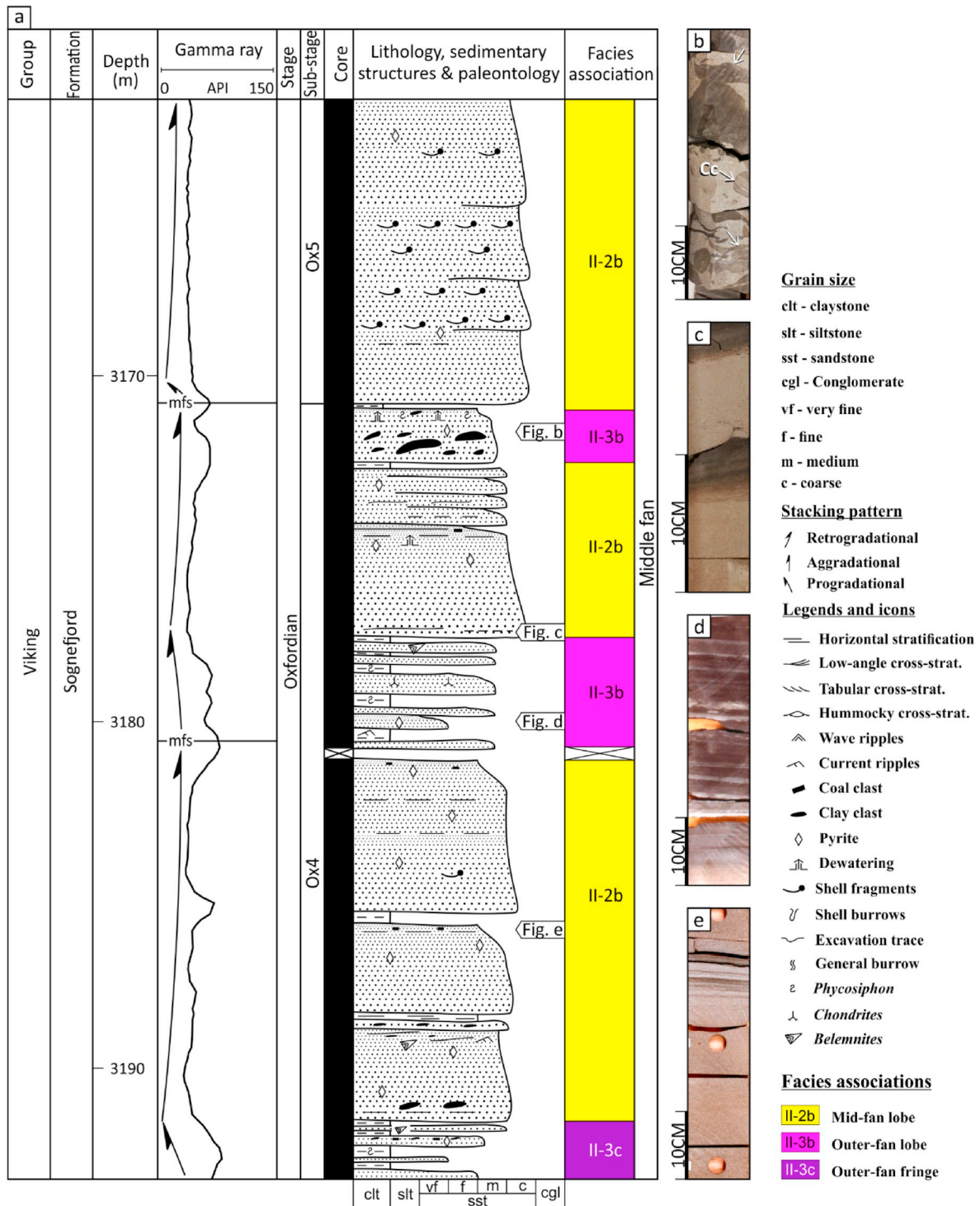


Fig. 8. Sedimentological logs of well 35/11-6 showing submarine stacking middle-inner fan facies associations. Well location in Fig. 2. Abbreviations: Cc, claystone clast as pointed by white arrows; F. A., facies association; mfs, marine flooding surface.

et al., 2018) or increased fault growth and linkage (cf. Cowie et al., 2000).

The lateral continuity of sandy units and facies variation from south to north indicate at least two major passages for submarine fan deposition: the Uer-Lomre terraces and the northern part of the Ryggsteinen Ridge (Fig. 11; Fig. 14). The northwest-directed gradual plunging and smooth facies variation with Facies Association II indicate that submarine fans developed towards the northwest (Fig. 9; Fig. 10; Fig. 15a).

## 5.2. Kimmeridgian

### 5.2.1. Well correlations

The top or base of the Kimmeridgian stage is usually absent (Figs. 9–11). No Kimmeridgian strata are reported in the area from wells 35/11-1 to 35/9-8 in the central part of the study area (Fig. 11). Therefore, the gross thickness of the preserved Kimmeridgian stage is usually less than 50 m.

The Kimmeridgian is dominated by moderate to high gamma-ray

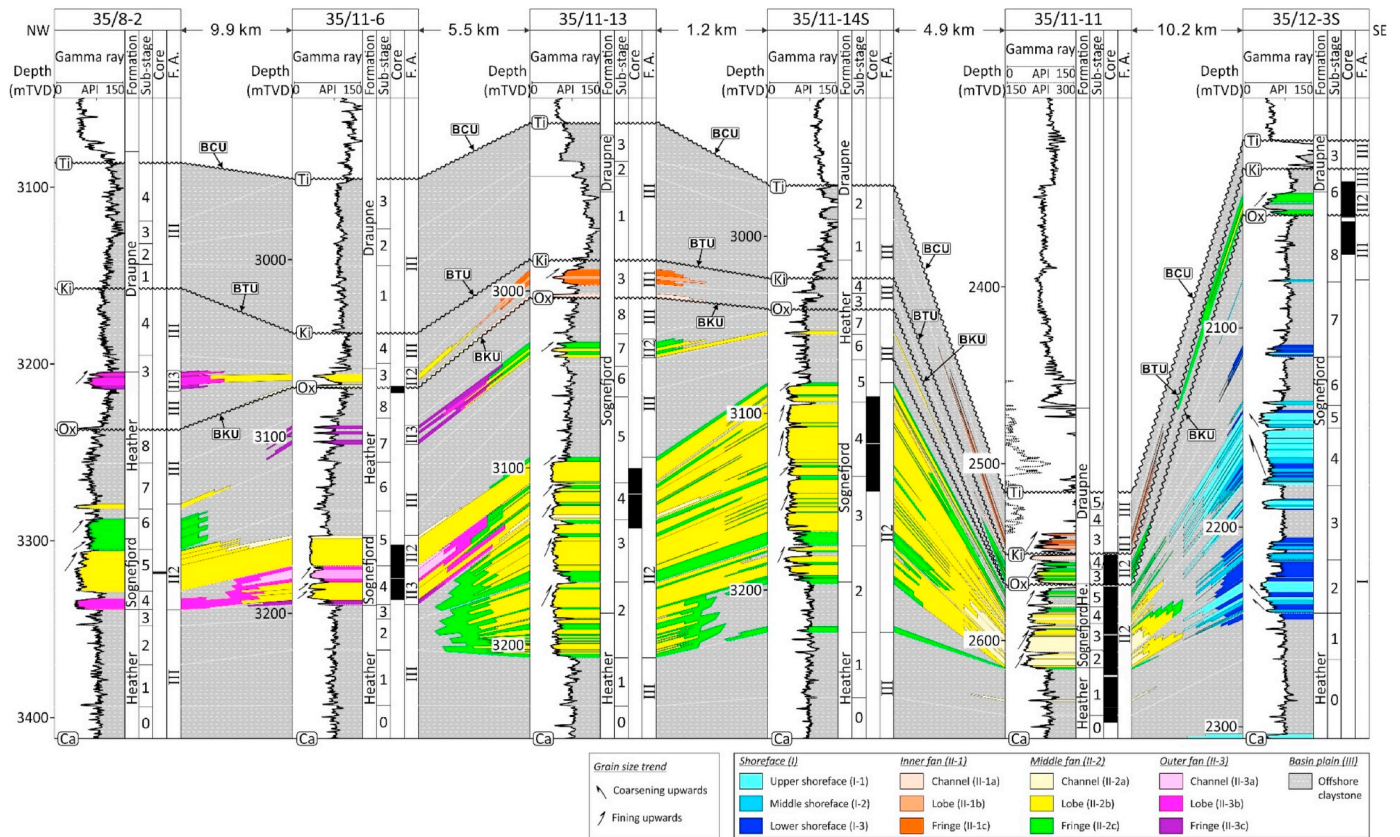


**Fig. 9.** Chronostratigraphic correlation with gamma-ray logs and facies association interpretation based on conventional core description from the Lomre Terrace (left) to the Uer Terrace (right). The section is flattened to the top of Callovian. Section location in Fig. 2. Abbreviations: BCU, Base Cretaceous Unconformity; BTU, Base Tithonian Unconformity; BKU, Base Kimmeridgian Unconformity; BOU, Base Oxfordian Unconformity; F.A., facies association; TVD, total vertical depth; Bj, Bajocian; Bt, Bathonian; Ca, Callovian; Ox, Oxfordian; Ki, Kimmeridgian; Ti, Tithonian.

values, indicative of shale (Figs. 9–11). However, in wells 35/11–13, 35/11–11, and 35/12–3S in the south to southeast, low gamma-ray values appear above hiatus of absent sub-stages (Fig. 9). In the southeasternmost well, 35/12–3S, the Kimmeridgian sandy units are dominated by Facies Association II-2 (middle fan). On the Lomre Terrace in the southwest, a westward transition occurs from facies association II-1 (well 35/11–13), via II-2 (well 35/11–6), to II-3 and III (well 35/8–2). In well 35/11–11 located in the south-central part of the study area, the Kimmeridgian Facies Association II-2 (middle fan) is overlain by Facies Association II-1 (inner fan). Sub-angular granules of claystone clasts are observed above distinct facies associations (Fig. 7).

### 5.2.2. Seismic data

The Kimmeridgian seismic sequence is usually unconformably overlain by the Tithonian sequence (Figs. 12–14). In addition to base Tithonian notches, prominent truncated features are observed in the hanging-wall block of the Vette Fault in the east (Fig. 17a) and in the area between the Ryggsteinen Ridge and the Måløy Slope (Fig. 17c). The truncated area around well 35/9–5 has a width of 6 km and reached 450 m deep.

### 5.2.3. Structural and thickness maps

The Kimmeridgian inherited the structures from the Oxfordian (Fig. 15b). However, in segments C2 and C3, an extensive area that covers the hanging-wall of major faults in the east commonly lacks Kimmeridgian strata. In the southwest of segment C2, the area where the Kimmeridgian sequence is absent aligns along a northwest-to-

southeast trend (Fig. 16b).

### 5.2.4. Interpretation

The Base Tithonian Unconformity is proposed to mark the unconformable Kimmeridgian–Tithonian contact (Figs. 9–14). The notches on seismic profiles and absent Oxfordian–Kimmeridgian in well logs are interpreted to be canyons as part of the Base Tithonian Unconformity. The canyons show an overall SE-to-NW orientation (Fig. 17; Fig. 18). Although rapid subsidence and antithetic faulting in immediate hanging-wall areas created extra accommodation space adjacent to Kimmeridge/Tithonian age extensional faults, less preservation of Oxfordian–Kimmeridge stages in the hanging-wall blocks indicates more submarine incision than a structural origin (Fig. 14; Fig. 17). Differently, the absence of Kimmeridgian sub-stages in the footwalls of basin-bounding faults, e.g. the Kinna Fault, is possibly related to subaerial erosion (Fig. 14).

The facies transition within Facies Association II (submarine fan) on the Lomre Terrace indicates sandy gravity flow deposition during the Kimmeridgian (Fig. 9). No significant Facies Association I (shoreface) is encountered in exploration wells (Figs. 9–11). Coincidentally, Facies Association II on the Lomre Terrace connects to the outlet of a submarine canyon (Fig. 11; Fig. 18).

## 5.3. Tithonian

### 5.3.1. Well correlations

The Tithonian is poorly preserved in the wells (Figs. 9–11). In

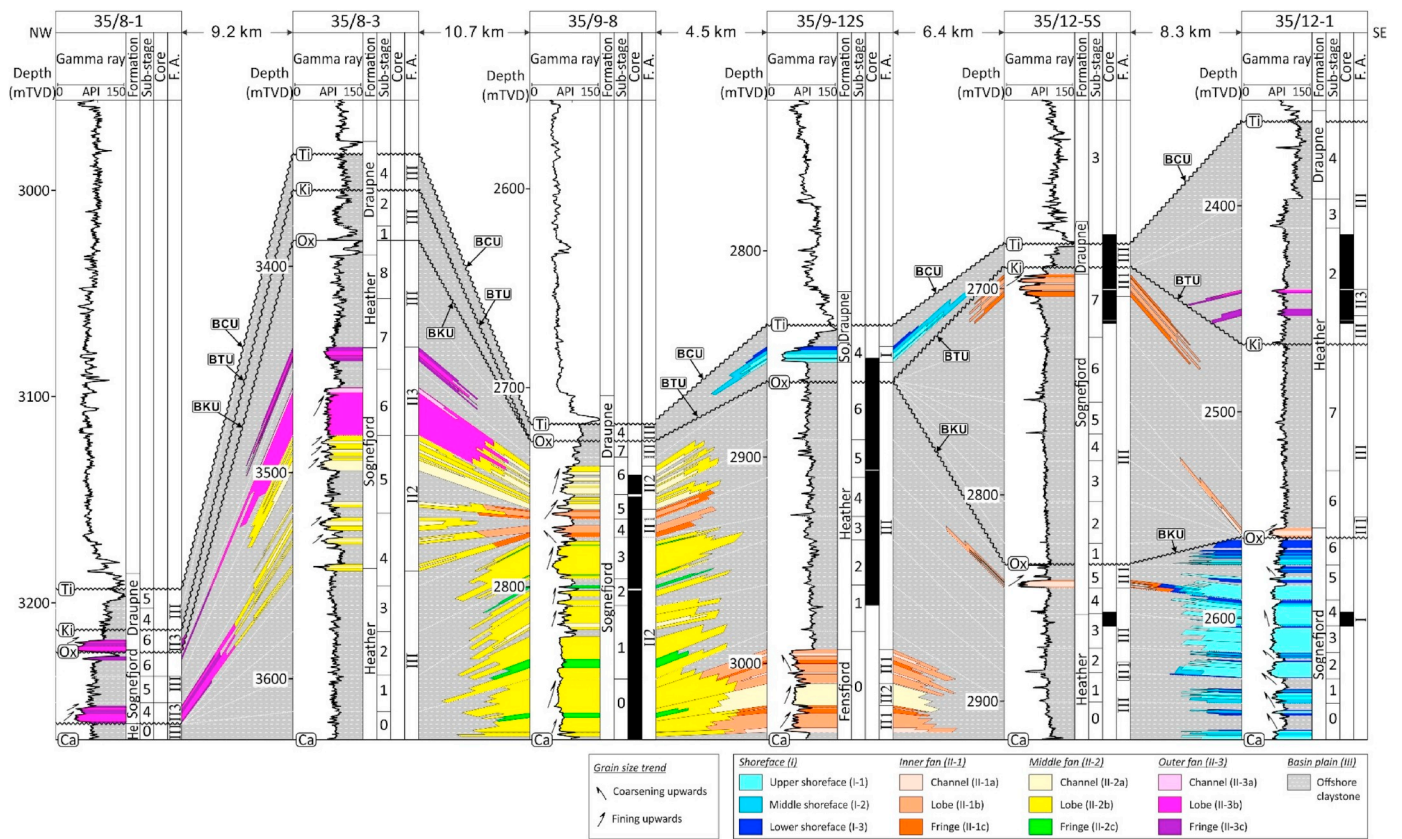


**Fig. 10.** Chronostratigraphic correlation with gamma-ray logs and facies association interpretation based on conventional core description from the Marflo Spur (left), via the Ryggsteinen Ridge, to the Uer Terrace (right). The section is flattened to the top of Callovian. Section location in Fig. 2. Abbreviations: BCU, Base Cretaceous Unconformity; BTU, Base Tithonian Unconformity; BKU, Base Kimmeridgian Unconformity; BOU, Base Oxfordian Unconformity; F.A., facies association; TVD, total vertical depth; Bj, Bajocian; Bt, Bathonian; Ca, Callovian; Ox, Oxfordian; Ki, Kimmeridgian; Ti, Tithonian.

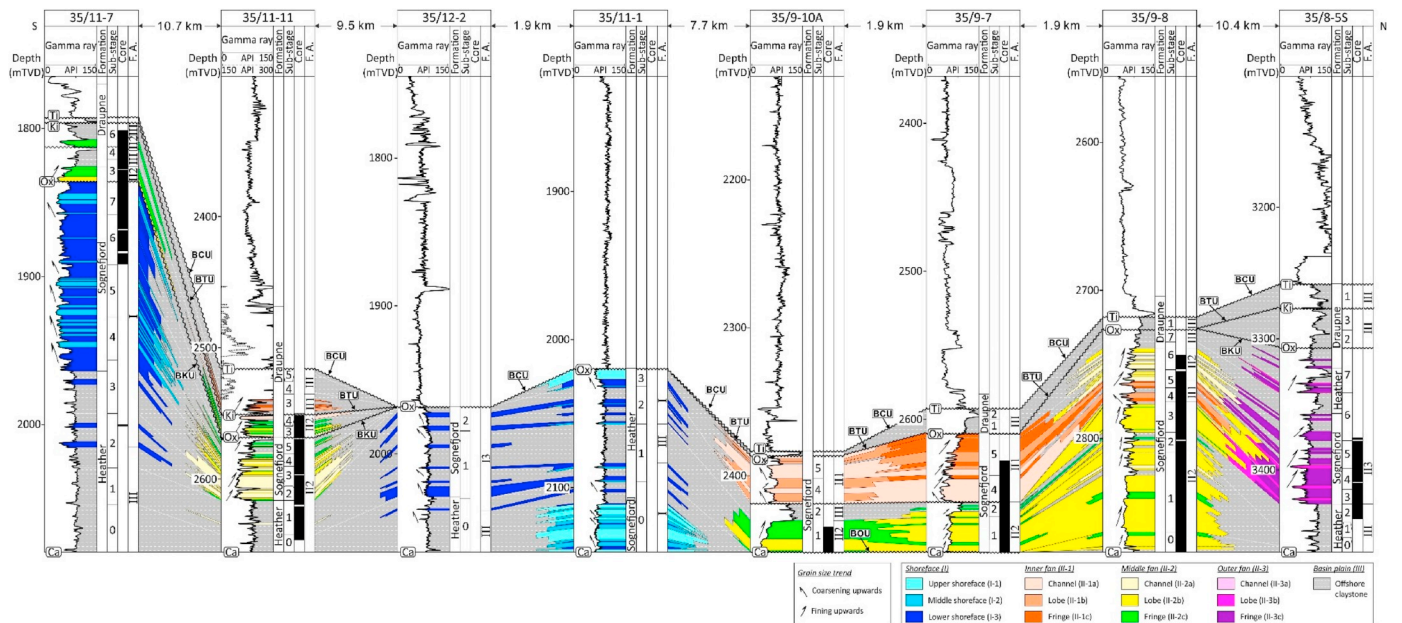


**Fig. 11.** Chronostratigraphic correlation with gamma-ray logs and facies association interpretation based on conventional core description from the Lomre Terrace (left), to the Ryggsteinen Ridge (right). The section is flattened to the top of Callovian. Section location in Fig. 2. Abbreviations: BCU, Base Cretaceous Unconformity; BTU, Base Tithonian Unconformity; BKU, Base Kimmeridgian Unconformity; BOU, Base Oxfordian Unconformity; F.A., facies association; TVD, total vertical depth; Bj, Bajocian; Bt, Bathonian; Ca, Callovian; Ox, Oxfordian; Ki, Kimmeridgian; Ti, Tithonian.

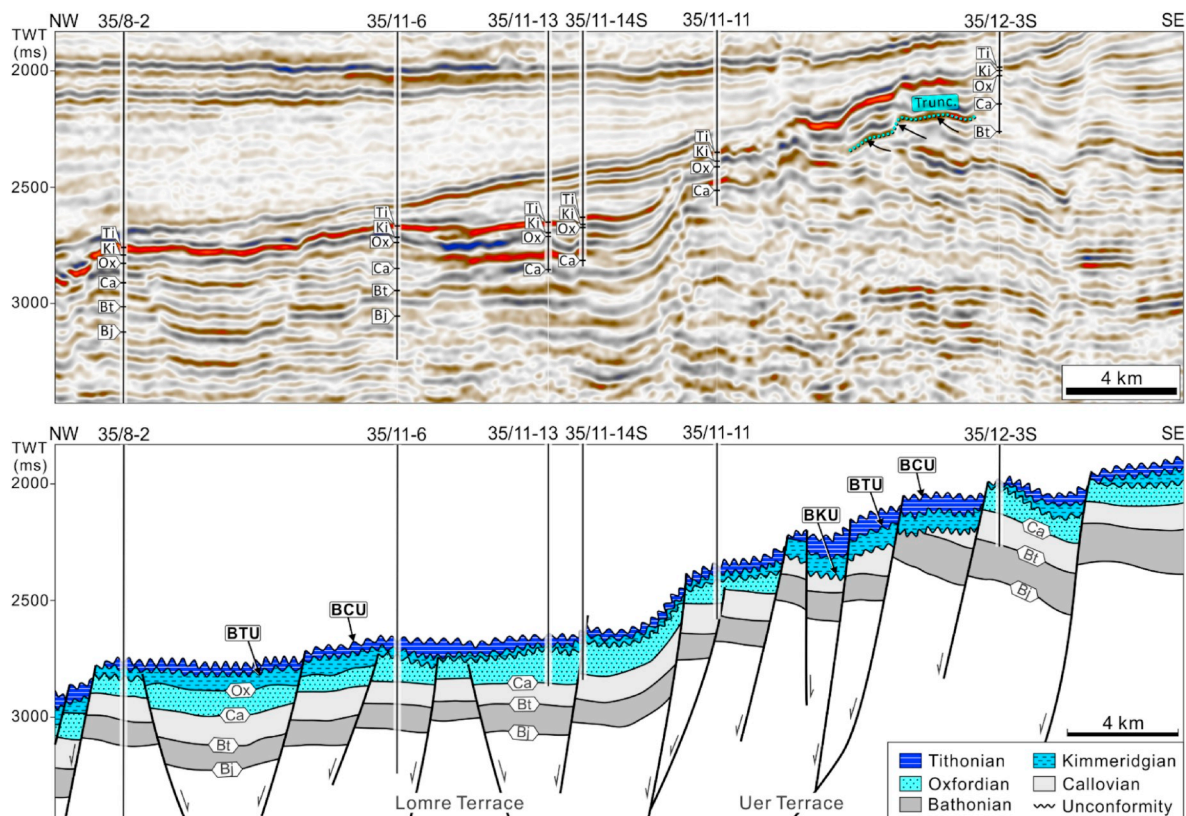


**Fig. 12.** Northwest-to-southeast seismic line showing Upper Jurassic stratigraphic patterns from the Lomre Terrace to the Uer Terrace. Section location in Fig. 2. The seismic profile is corresponding to well section in Fig. 9. Abbreviations: TWT, two-way-time; Bj, Bajocian; Bt, Bathonian; Ca, Callovian; Ox, Oxfordian; Ki, Kimmeridgian; Ti, Tithonian; BCU, Base Cretaceous unconformity; BTU, base Tithonian unconformity; BKU, base Kimmeridgian unconformity.

general, the Tithonian is dominated by Facies Association III (offshore claystone) showing high to very high ( $> 150$  API) gamma-ray values, but occasionally interbedded with isolated sandy units. In well 35/9-12S in the center of the study area, a 34 m-thick sandy package belongs to Facies Association I (shoreface; Fig. 10). However, well 35/12-1 contains thin-layered sandy units of Facies Association II-2c (outer fan; Fig. 10; core photos are available in NPD, 2019).

### 5.3.2. Seismic data

Seismic reflectors for the Bathonian–Oxfordian are truncated by the Tithonian horizon (Figs. 13 and 14). Along the western margin of the Ryggsteinen Ridge, the Tithonian seismic sequence is absent (Fig. 14).

### 5.3.3. Structural and thickness maps

The Tithonian structures were inherited from the Oxfordian and Kimmeridgian sequences (Fig. 15c). The Tithonian depocenters were mainly developed in the hanging-wall blocks of major faults and the complete absence of the Tithonian stage is limited to the footwall blocks of major faults (Fig. 16c).

### 5.3.4. Interpretation

The development of significant amounts of Facies Association III (offshore claystone) indicates a regional-scale flooding event (cf. Jacquín et al., 1998; Stow et al., 2001) that submerged areas that were exposed during the Kimmeridgian (Fig. 15; Fig. 16). The major unconformities on top of the Tithonian stage are assigned to the Base Cretaceous Unconformity (cf. Ziegler, 1975; Nottvedt et al., 1995) that is likely related to erosion accompanied by footwall uplift during the Early Cretaceous (Figs. 12–15).

## 6. Discussion

### 6.1. Depositional evolution of Upper Jurassic shoreface to deep-water systems in a segmented rift system

#### 6.1.1. Lower Oxfordian (Ox0–2; spans 1.4 my)

The lower Oxfordian constitutes shoreface facies associations along an NE–SW-oriented coastline (Fig. 19a; cf. Zhong and Escalona (in press)). Sub-aqueous drainage entry points are located in the eastern part of segment C2, which was determined by first-order rift segmentation (Zhong and Escalona (in press)). Three large-scale notches identified from 3D seismic data are interpreted to represent submarine canyons which acted as feeder systems of submarine fans:

- (1) The southernmost canyon proceeded several kilometers along the Horda–Uer Fault Transfer Zone in an ENE–WSW direction before being captured by the NNW-oriented oblique-slip segment of the Kinna Fault (Fig. 18). Channelized turbidites subsequently developed in a submarine fan on the Lomre Terrace with fan lobes spanning around 16 km in length and 14 km in width (Fig. 19a).
- (2) The middle canyon entered the interaction area between the Vette Fault segments (Fig. 18). Due to the development of NNW–SSE-striking oblique-slip faults, the canyon was deflected to the north-northwest. A submarine fan (ca.  $12 \times 6$  km) was developed along Ryggsteinen–Sogn fault transfer zone (Fig. 19a).
- (3) The northernmost canyon entered from the central-eastern part of the study area, where there is a lack of major faults (Fig. 18). A submarine fan (ca.  $10 \times 3$  km) developed across the Ryggsteinen–Sogn fault transfer zone (Fig. 19a).

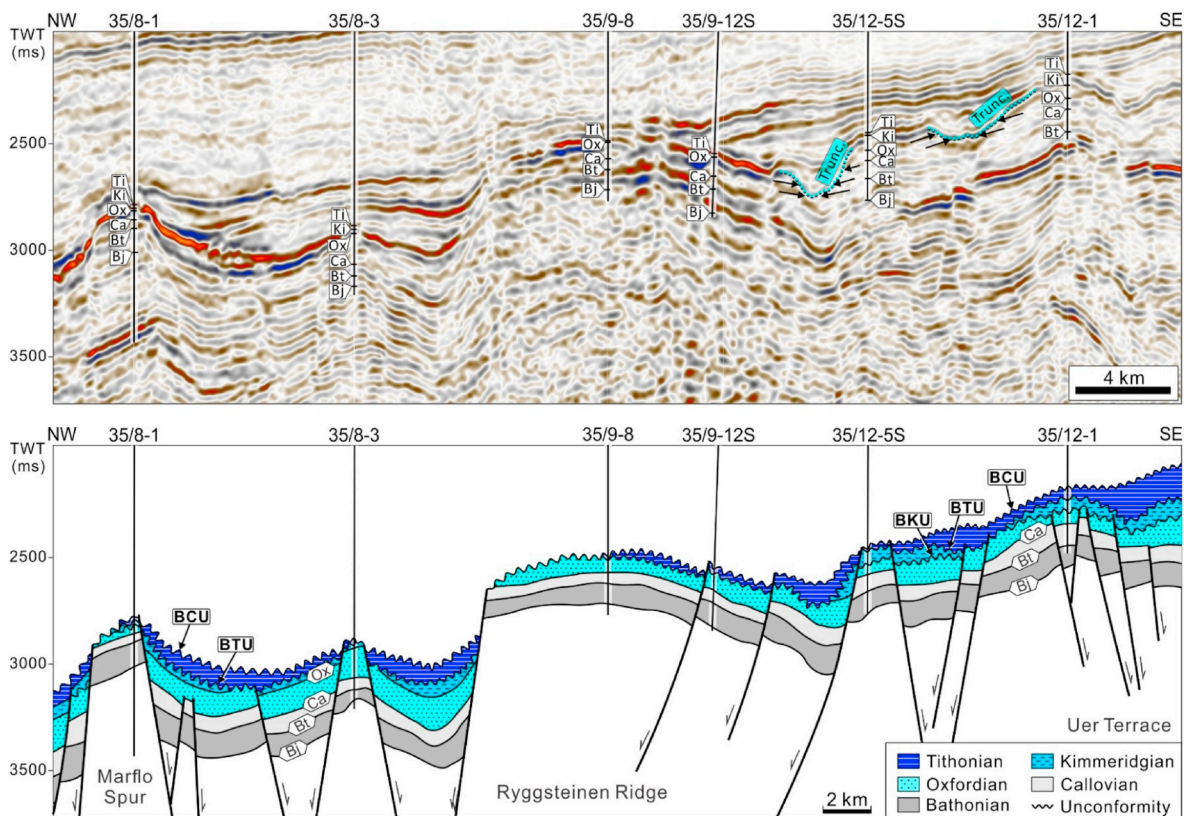


**Fig. 13.** Northwest-to-southeast seismic line showing Upper Jurassic stratigraphic patterns from the Marflo Spur, via the Ryggsteinen Ridge, to the Uer Terrace. Section location in Fig. 2. The seismic profile is corresponding to well section in Fig. 10. Abbreviations: TWT, two-way-time; Bj, Bajocian; Bt, Bathonian; Ca, Callovian; Ox, Oxfordian; Ki, Kimmeridgian; Ti, Tithonian; BCU, Base Cretaceous unconformity; BTU, base Tithonian unconformity; BKU, base Kimmeridgian unconformity.

### 6.1.2. Middle Oxfordian (Ox3–5; spans 1.5 my)

The Middle Oxfordian deposition resulted in an overall progradational succession (Facies association 1) and the development of extensive submarine fans (Facies Association II; Fig. 9; Fig. 10; Fig. 19b). At the Lomre Terrace, the axial and transversal extension of fan lobes reached approximately 22 km and 20 km respectively (Fig. 19b). Coarse-grained decimeter-scale Bouma sequences in the middle fan (Facies Association II-2; Fig. 7) indicate that sandy gravity flows evolved into high-density turbidity currents (cf. Kneller and Branney, 1995; Leclair and Arnott, 2005; Cantero et al., 2012). By contrast, fine-grained decimeter-to centimeter-scale rhythmic sequences in the outer fan (Facies Association II-3; Fig. 8) are related to low-density turbidity currents (cf. Bouma, 1962; Mulder et al., 2001; Herbosch and Verniers, 2014). The matrix supported conglomerates within the outer-fan lobe (Facies Association II-3b) may be a hybrid bed (Fig. 8b) with material from cohesive debris flow and cohesionless turbidity flow (cf. Hodgson, 2009; Spsychala et al., 2017). The cohesive debris flow may have originated as a localized failure of an unstable or unconsolidated Kinna-Fault scarp (Fig. 19b).

In the area of well 35/8-2 in the west, the sandy units are interpreted to form part of a suprafan lobe that was initiated by active submarine channels that incised older turbidite lobes (Fig. 19b; cf. Piper and Normark, 1983; Shanmugam and Moiola, 1991; Galloway, 1998). Based on well log characters, core sedimentology, and biostratigraphic data, the middle- and outer-fan successions (facies associations II-2 and II-3) in well 35/8-2 can be correlated to shoreface packages (Facies Association I) in well 35/12-3S further to the southeast (Fig. 9), suggesting an NW-directed source-to-sink relationship from shallow-marine to deep-water environments.

Near the Ryggsteinen-Sogn fault transfer zone, submarine fans

prograded about 25 km into the basin (Fig. 19b). In the northern part of the Ryggsteinen Ridge, the clast-supported conglomerate layers that are occasionally mixed with matrix-supported conglomerate (Figs. 6 and 11) indicates that the inner-fan cohesionless-debris flow regime was intervened by cohesive debris flows (cf. Nemeč and Steel, 1984; Postma, 1986; Mulder and Alexander, 2001).

### 6.1.3. Upper Oxfordian (Ox6–8; spans 2.2 my)

The sedimentation was dominated by retrogradation of the shoreface (Facies Association I; Figs. 9, 10 and 19c). The scale of submarine fans decreased with the axial and transversal extension of fan lobes on the Lomre Terrace decreasing from 22 × 20 km to 16 × 14 km (Fig. 19c). At the Ryggsteinen-Sogn fault transfer zone, channelized turbidite complexes in different submarine fans started to merge and formed a complex channel-lobe system. Merging of submarine fans was likely the result of rift segmentation and the role it played in controlling border fault growth and linkage (cf. Zhong and Escalona (in press)).

### 6.1.4. Kimmeridgian (Ki1–7; spans 4.0 my)

Shoreface deposits developed at the rims of exhumed structural highs that emerged due to the interplay of rift segmentation and fault linkage (Fig. 19d; Zhong and Escalona (in press)). Multiple submarine canyons were developed near the Vette Fault (Fig. 18). The development of NNW-SSE-striking oblique-slip faults forced pre-existing canyons. The canyons were deflected towards the north (Zhong and Escalona (in press)). Furthermore, due to footwall uplift of the Kinna Fault, pre-existing canyon across the Ryggsteinen Ridge were abandoned (Fig. 14). Retreated canyon deflected towards the north to form major canyons by eroding both the sea floor and the Ryggsteinen-Sogn fault transfer zone (Fig. 17; Fig. 18; Fig. 19d). In the southeastern

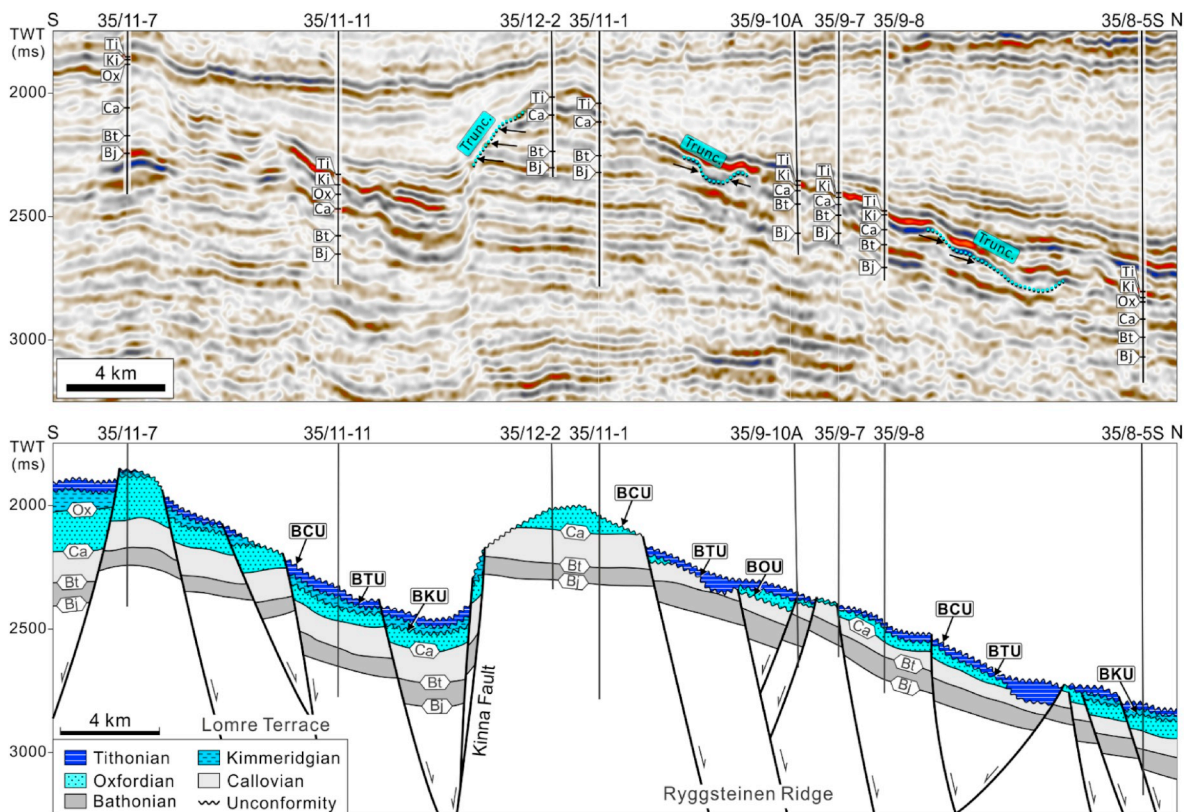


Fig. 14. South-to-north seismic line showing Upper Jurassic stratigraphic patterns from the Lomre Terrace to the Ryggestein Ridge. Section location in Fig. 2. The seismic profile is corresponding to well section in Fig. 11. Abbreviations: TWT, two-way-time; Bj, Bajocian; Bt, Bathonian; Ca, Callovia; Ox, Oxfordian; Ki, Kimmeridgian; Ti, Tithonian; BCU, Base Cretaceous unconformity; BTU, base Tithonian unconformity; BKU, base Kimmeridgian unconformity; BOU, based Oxfordian unconformity.

margin of the Sogn Graben, the distribution of major faults (Fig. 15a) and NW-directed canyons (Fig. 18) connect to major submarine fans, indicating that submarine canyons have controlled sediment dispersal (Fig. 11). On the Lomre Terrace, a 10-km-wide submarine fan lobe prograded up to 15 km into the basin (Fig. 19d). The claystone clasts in well 35/11-11 are texturally and mineralogically immature (Fig. 7b, e). They are envisaged to be locally derived from the adjacent Ryggestein Ridge, which can be referred from the intra-Draupne submarine fan reservoirs in the Johan Sverdrup area, southern North Sea (cf. Scott and Ottesen, 2018).

#### 6.1.5. Tithonian (Ti1–6; spans 5.0 my)

Tithonian deposition is dominated by offshore claystone (Facies Association III) due to regional flooding (cf. Jacquin et al., 1998; Stow et al., 2001). Shoreface sand (Facies Association I) was deposited at the edge of exhumed structural highs, for example well 35/9-12S at the edge of the Ryggestein Ridge (Fig. 10; Fig. 19e). Occasional submarine fans (Facies Association II) developed for example in the area of well 35/11-11 (Fig. 19e).

#### 6.2. Depositional variations between non-segmented and segmented rift systems

In non-segmented rift systems, syn-rift deposition and stratigraphic architectures are determined by the development and interaction of rift-border faults. Relay zones and non-relay overlaps commonly act as the conduits that allow axial ramp drainage toward the inboard and outboard hanging walls (Gawthorpe and Hurst, 1993; Leeder, 1993;

Peacock and Sanderson, 1994; Gawthorpe and Leeder, 2000). Sandy gravity flows are able to bypass the relay zones to establish submarine fans that are in general sub-parallel to the strike of border faults (Fig. 20a). In the Brae Field area, southern North Sea, back-tilting of border-fault footwalls and footwall uplift created emergent source areas adjacent to grabens (cf. Allerton et al., 2018). Therefore, border faults are preferable locations to explore for reservoir quality sandstones in non-segmented rift systems.

In contrast, the boundaries of segmented rift systems behave as weak structures that allow the entering and bypassing of regional drainages (Fig. 20b; cf. Sleep and Blanpied, 1992). For example, in the Gulf of Corinth, river valleys or submarine canyons developed along transfer fault zones building up Gilbert-type fan deltas at the outlets (Poulimenos et al., 1993; Zhong et al., 2018). In the study area, during the Oxfordian–Kimmeridgian, segmentation took place modifying the drainage system into a point source (cf. Zhong and Escalona (in press)). At the end of the Kimmeridgian, the entry points particularly concentrated near the Horda–Uer transfer fault zone (HUFTZ; Fig. 18). From the Uer Terrace to the Lomre Terrace, it is clear that the boundary of first-order rift segmentation, instead of rift-border faults, is a favorable location to explore good reservoir-quality sandstones (Fig. 18; Fig. 19a–d; Fig. 20b). At the Ryggestein–Sogn transfer fault zone (RSTFZ), absence of Upper Jurassic sequences in the eastern part made it uncertain to speculate the impact of the first-order rift segmentation on sediment dispersal (Fig. 15; Fig. 16). However, concentrated submarine fan sandstones in the northern flank of the Ryggestein Ridge connect to the NW-directed canyons, suggesting the potential influence of second-order rift segmentation on sediment dispersal (Fig. 11;

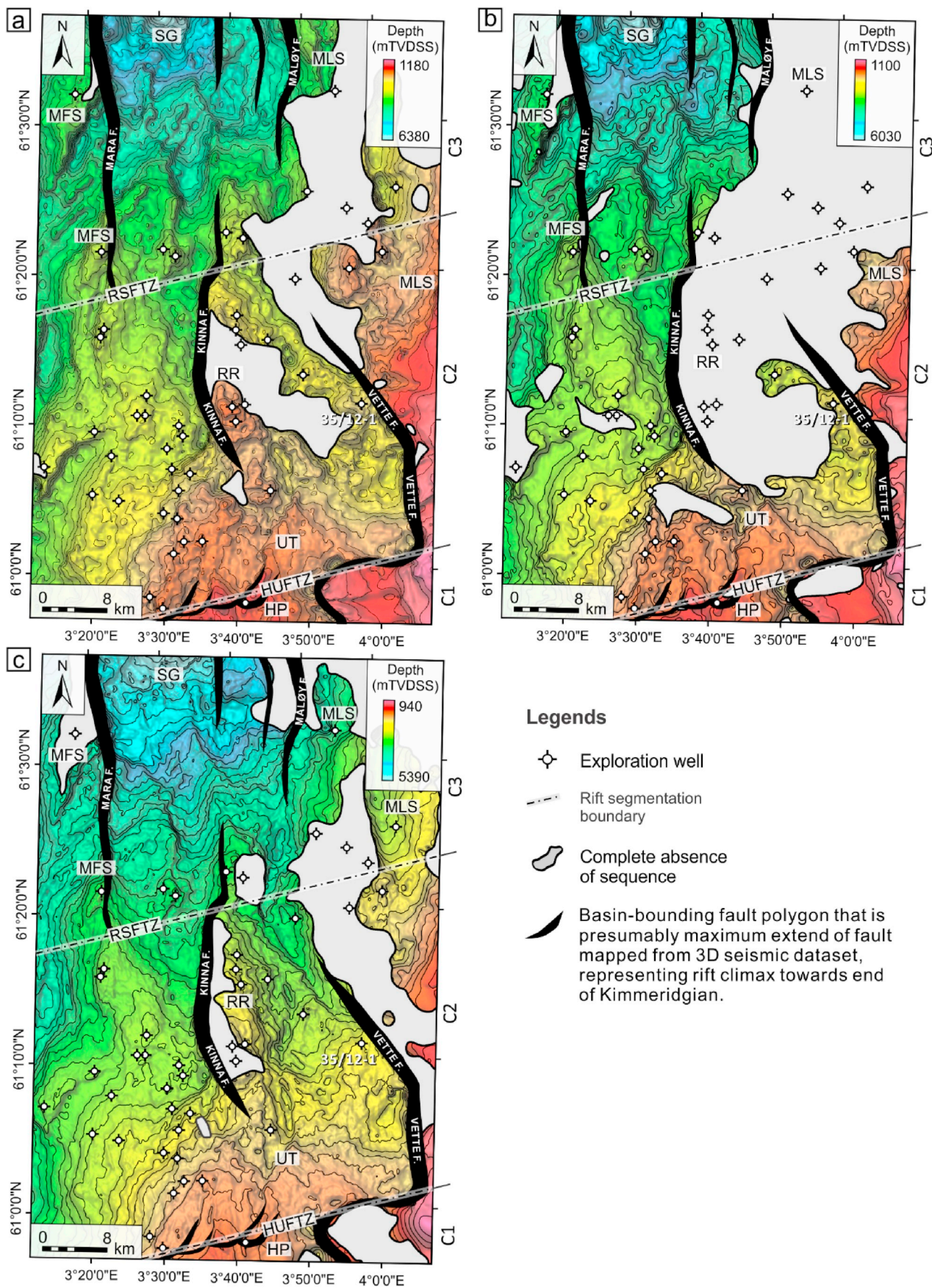
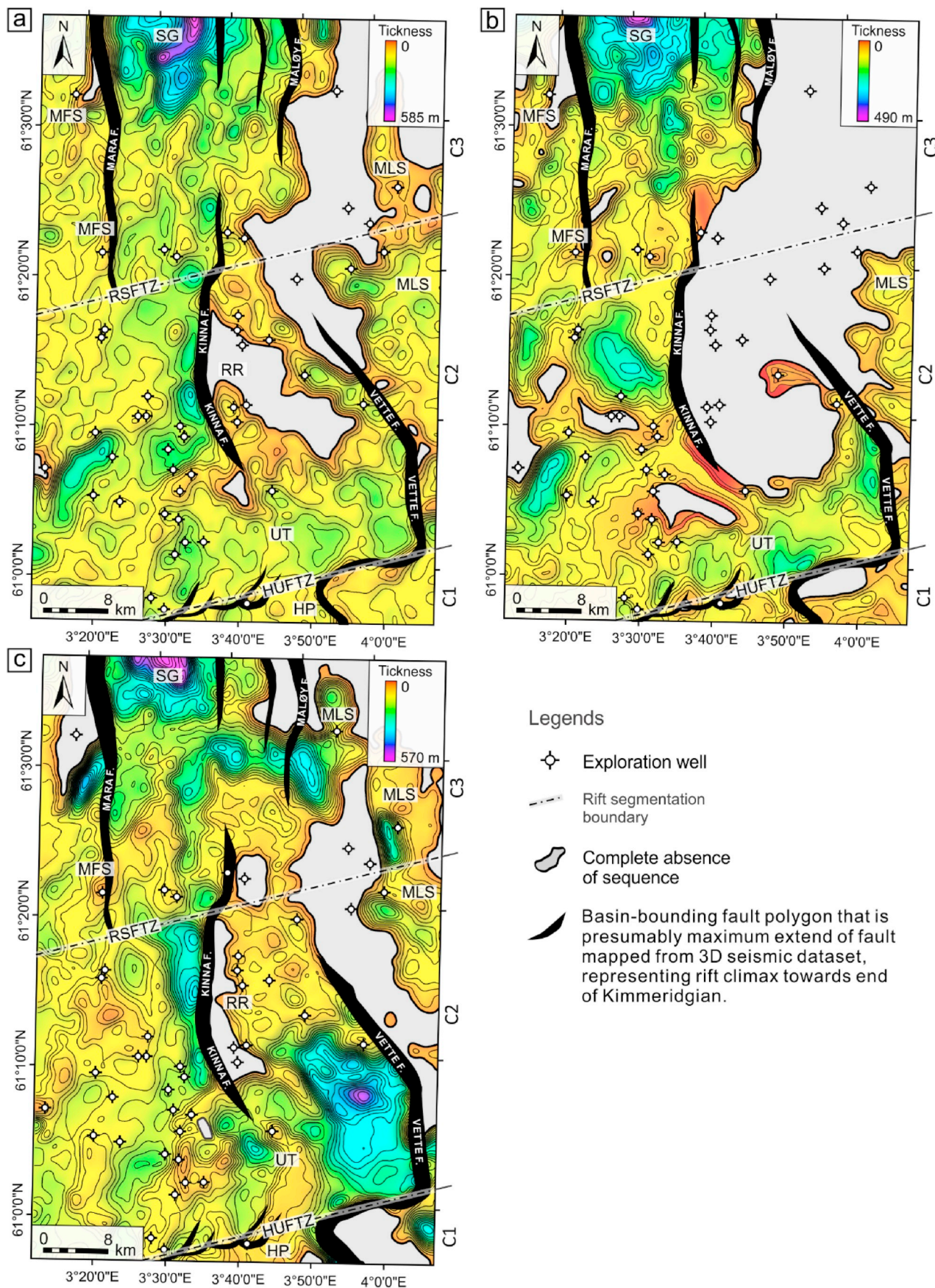


Fig. 15. Structural maps of the top Oxfordian (a), top Kimmeridgian (b), and top Tithonian (c) horizons. Grey polygons illustrate the areas that are eroded or affected by non-deposition. Abbreviations: HP, Horda Platform; HUFTZ, Horda-Uer Fault Transfer Zone; LT, Lomre Terrace; MFS, Marflo Spur; MLS, Måløy Slope; RR, Ryggsteinen Ridge; RSFTZ, Ryggsteinen-Sogn Fault Transfer Zone; SG, Sogn Graben; UT, Uer Terrace; F., fault.



**Fig. 16.** The thickness maps for preserved Oxfordian (a), Kimmeridgian (b), and Tithonian (c) stages. Abbreviations: HP, Horda Platform; HUFTZ, Horda–Uer Fault Transfer Zone; LT, Lomre Terrace; MFS, Marflo Spur; MLS, Måloy Slope; RR, Ryggsteinen Ridge; RSFTZ, Ryggsteinen–Sogn Fault Transfer Zone; SG, Sogn Graben; UT, Uer Terrace; F., fault.

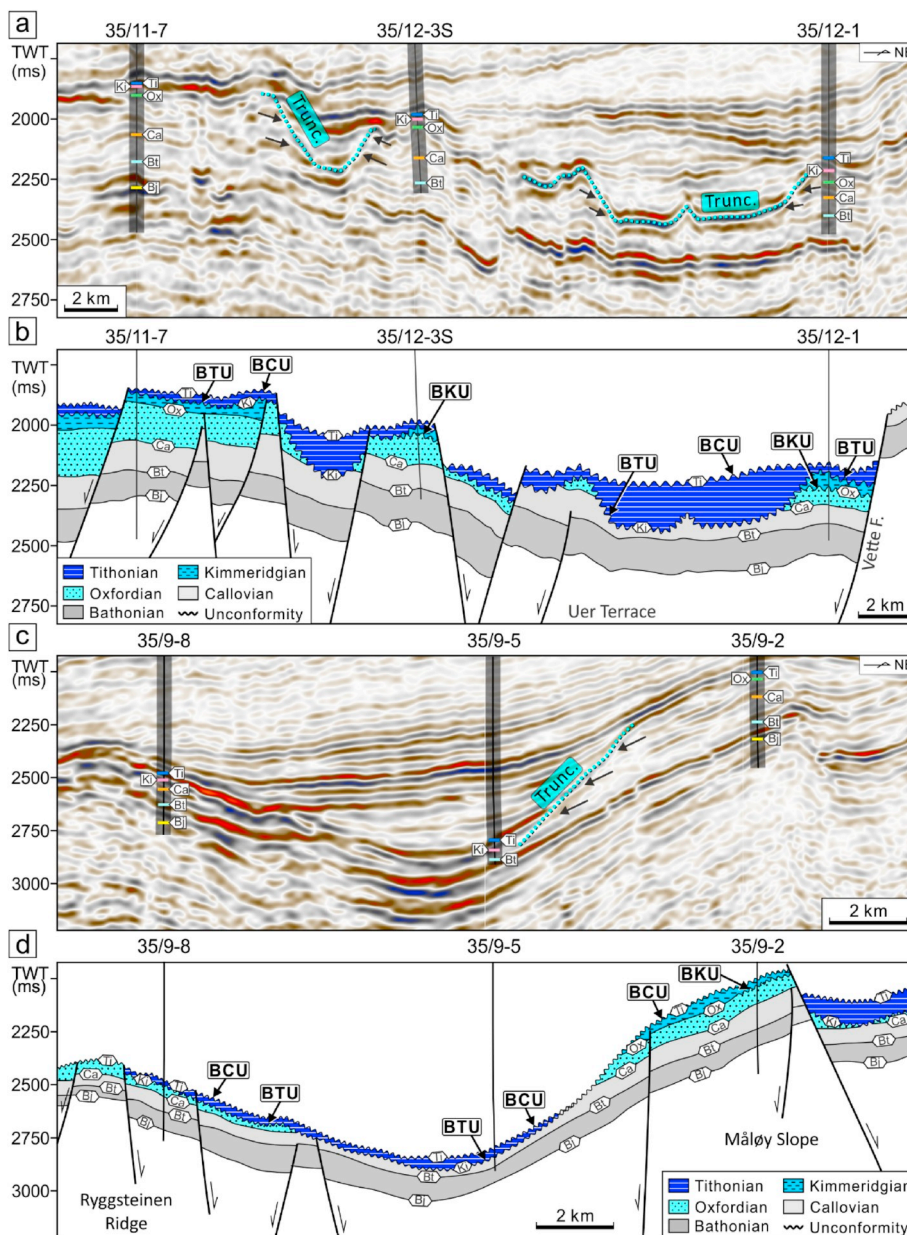


Fig. 17. Southwest-to-northeast seismic lines showing the Base Tithonian Unconformity created by erosion of submarine canyons. Section locations in Fig. 18. Abbreviations: BCU, Base Cretaceous Unconformity; BTU, Base Tithonian Unconformity; BKU, Base Kimmeridgian Unconformity; Bj, Bajocian; Bt, Bathonian; Ca, Callovian; Ox, Oxfordian; Ki, Kimmeridgian; Ti, Tithonian.

Fig. 14). Besides, the route of submarine canyon feeder system can be modified due to the development of oblique-slip faults (cf. Zhong and Escalona (in press)), which led to the deposition of submarine fans with a strike parallel to the regional extension (Fig. 18; Fig. 19; Fig. 20b). Thus, the impact of the second-order rift segmentation should be considered when determining sedimentary architecture of sandy gravity flow deposits within individual rift segments.

In addition, mineralogically immature claystone clasts in the hanging-wall of the Kinna Fault indicate that Permo-Triassic fault reactivation is able to control the temporal and spatial development of syn-rift turbidite systems, as discussed by the previous studies in the South Viking Graben (Jackson et al., 2011) and the central North Sea

(McArthur et al., 2016).

### 7. Conclusions

Upper Jurassic successions in the North Sea provide an example of shoreface to submarine fan depositional systems. The fans were mainly fed by regional drainage that originated from inland rift margins. The facies architecture and genetic evolution of submarine fans reveal the evidence of tectono-sedimentary processes in a segmented rift system, which is considerably different from non-segmented rift systems. It is concluded that:

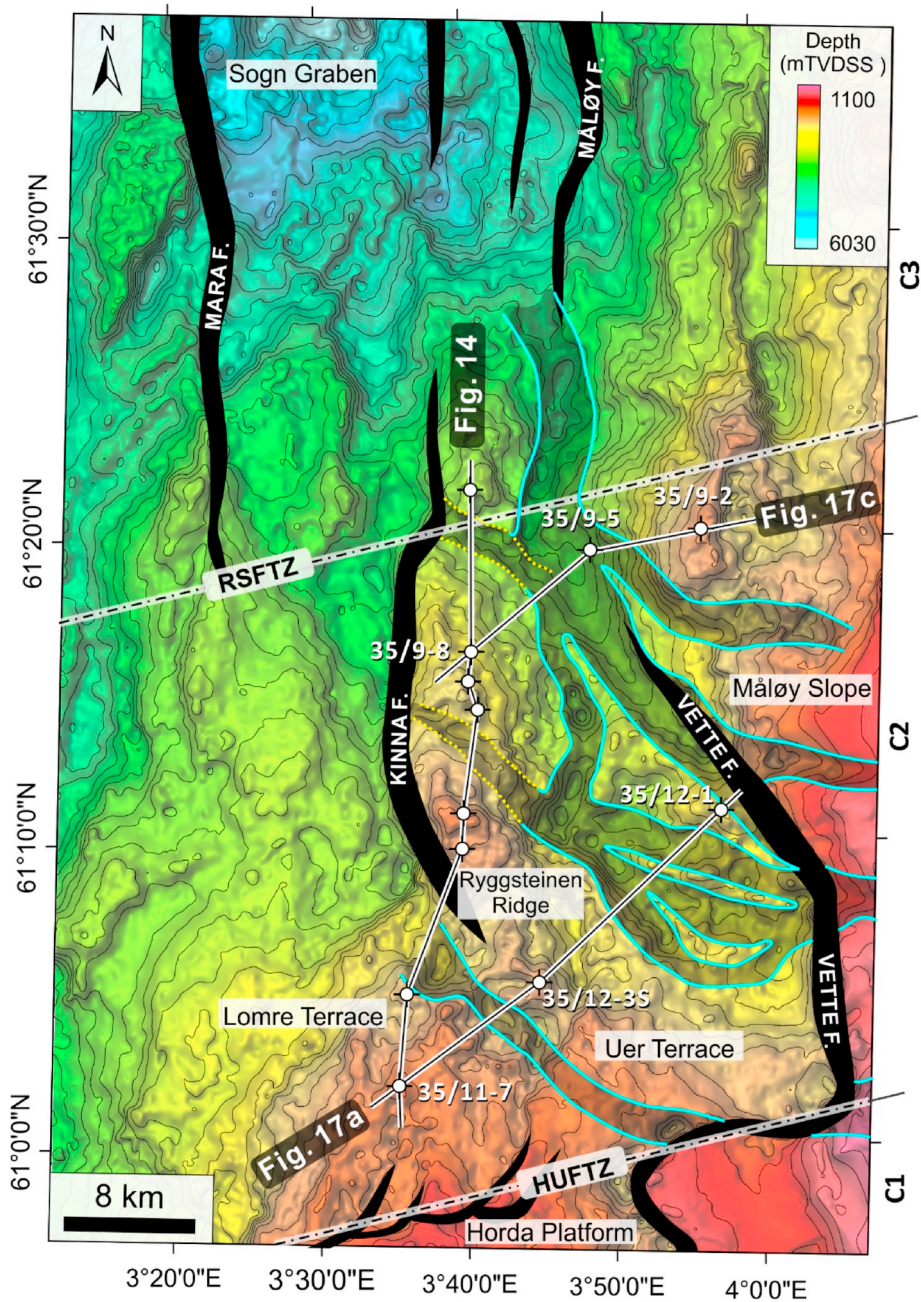


**Fig. 18.** Structural map of the Base Tithonian Unconformity. Notes: (1) light-blue lines are proposed boundary of submarine canyons; (2) yellow dotted line show the Oxfordian canyons that were abandoned during the Kimmeridgian; and (3) fault polygons are marked for basin-bounding faults only. Abbreviations: HUFTZ, Horda–Uer Fault Transfer Zone; RSFTZ, Ryggsteinen–Sogn Fault Transfer Zone. (For interpretation of the references to colour in this figure legend, the reader is referred to the Web version of this article.)

- (1) Deep-water submarine fans within the study area demonstrate significant erosion, channel fill, and coarse-grained deposits. This indicates the ability of submarine canyons to erode the sea floor as the result of rift segmentation. Regional drainages transported coarse material for over 30 km with channelized turbidites deposited towards the upper section of the submarine canyons.
- (2) Rift segmentation exerted substantial impact on the generation, modification, and abandonment of submarine canyons. The internal

architecture and spatial distribution of submarine fans reflect changes in the paleogeography and feeder conduits. The locations for entry of regional drainage and sandy gravity-flow deposition are controlled by first-order rift segmentation along transfer fault zones, whereas the route of submarine canyon feeder system and the orientation of submarine fan lobes are determined by second-order rift segmentation along oblique-slip faults.

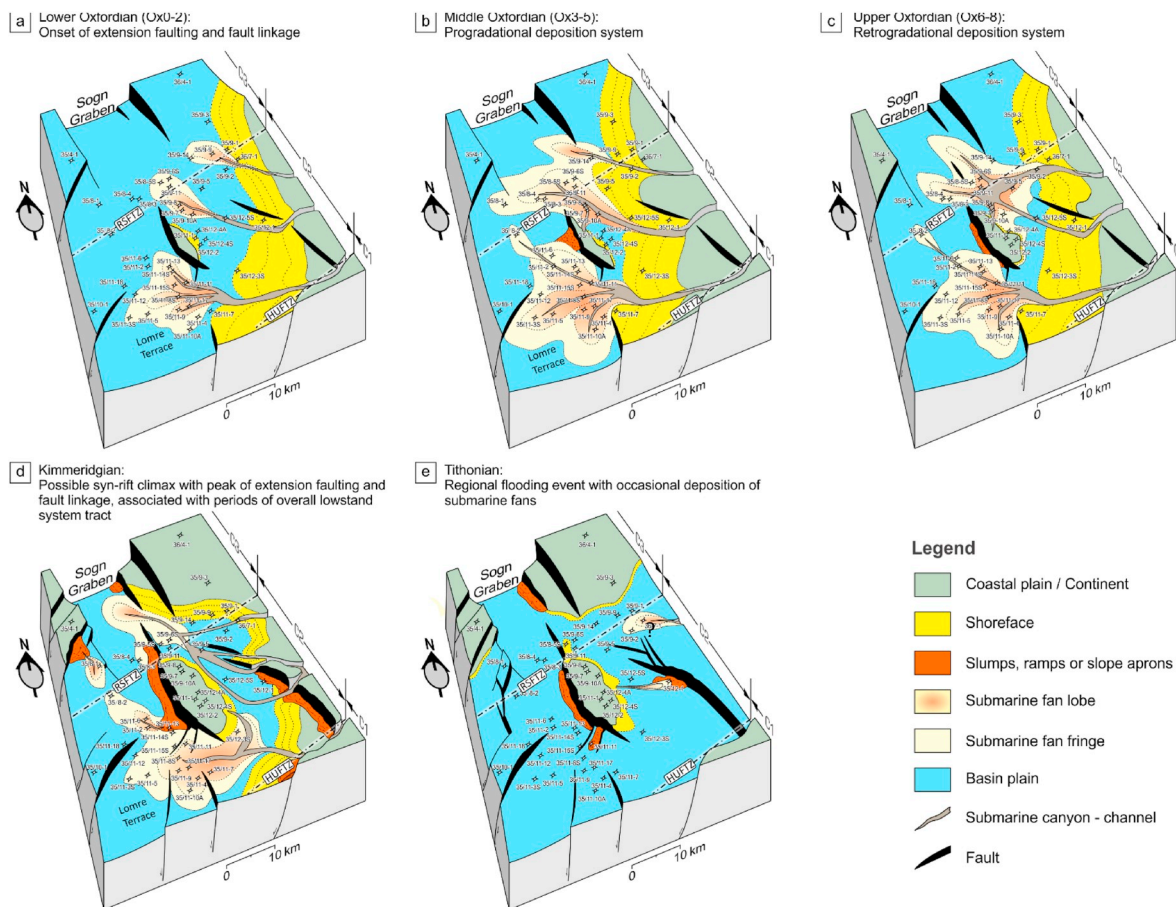


Fig. 19. Proposed block diagrams showing the drainages, facies architectures, and depositional system evolution. Abbreviations: HUFTZ, Horda–Uer Fault Transfer Zone; RSFTZ, Ryggsteinen–Sogn Fault Transfer Zone.

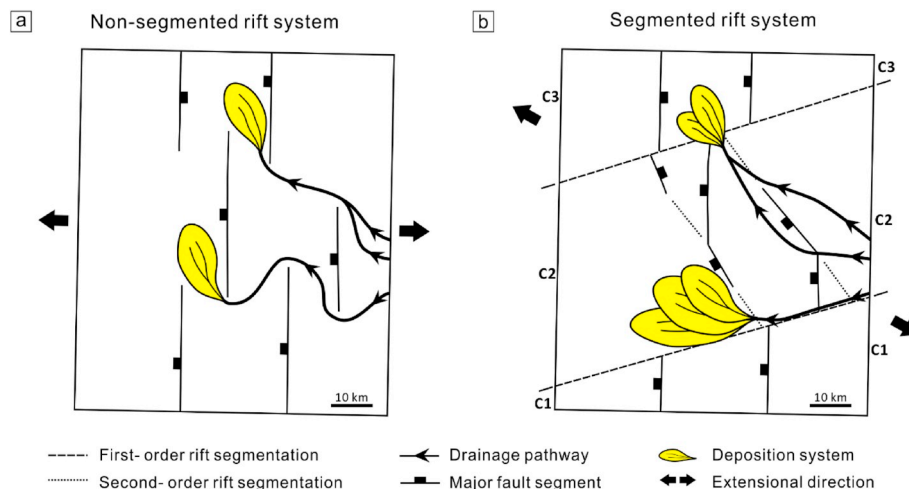


Fig. 20. Comparison of drainages, facies architectures, and depositional system between segmented (a) and non-segmented (b) rift systems.

**CRediT authorship contribution statement**

**Xiaoan Zhong:** Formal analysis, Investigation, Writing - original draft. **Alejandro Escalona:** Conceptualization, Methodology, Writing - review & editing. **Carita Augustsson:** Supervision, Writing - review & editing.

**Declaration of interests**

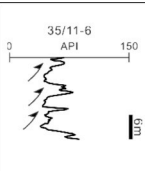
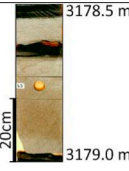
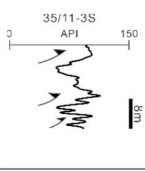
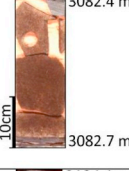
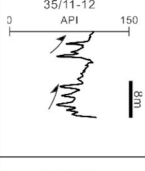
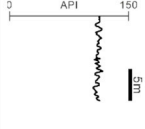
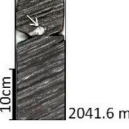
The authors declare that they have no known competing financial interests or personal relationships that could have appeared to influence the work reported in this paper.

**Table 1**  
Lithological facies classification and interpretation of Upper Jurassic syn-rift deposits.

Facies associations				Gamma-ray pattern	Conventional core	Lithology	Description	Interpretation
1st-order	2nd-order	3rd-order	Label					
Shoreface	Upper		I-1			Cross-stratified coarse-grained sandstone	Decimeter- to meter-scale beds of moderately well sorted, medium- to coarse-grained, quartz-rich sandstone. Cross-stratification is defined by silty drapes. Rare and sparse bioturbation with burrows are found. Shell fragments of mixed assemblage are locally observed.	Shoreface deposits with local bioturbation during fair-weather conditions.
	Middle		I-2			Cross-laminated medium-grained sandstone	Moderately well to locally poorly sorted, medium-grained, slightly silty sandstone. Decimeter-scale sandstone layers display ripple to medium-scale cross stratification and diffuse mottled fabric towards the top. Bioturbation is sporadic.	
	Lower		I-3			Bioturbated or hummocky laminated fine-grained sandstone	Well sorted, fine-grained, quartz-rich to slightly silty sandstone. Centimeter- to decimeter-scale beds with swaley or hummocky cross-stratification. Weak to locally moderate bioturbation with burrows, escape traces, etc. <i>Chondrites</i> and <i>Schaubcylindrichmus</i> are observed.	
Submarine fan	Inner	Channel	II-1a			Amalgamated inverted-to-normally graded conglomerate	Meter-scale amalgamated beds of clast-supported pebbly conglomerates with erosive bases, grading up into moderately to well sorted, pebbly, medium-grained, quartz-rich sandstone. The matrix comprises moderately sorted, quartz-rich, medium- to coarse-grained sand. Inverted graded clasts at the bottom are sub-horizontally aligned pebbles and cobbles of laminated mudstone and cemented sandstone. Shell fragments are locally observed.	Gravity-driven mass transport of coarser-grained sediments within submarine fan systems.
		Lobe	II-1b			Mudstone-clast entrained and corroded structureless / normal-graded sandstone beds	Decimeter-scale beds of moderately-to-well sorted, medium-grained to pebbly sandstone. Sandstones are structureless or displays normal-graded planar lamination. Abundant claystone clasts of cemented sandstones are found.	
		Fringe	II-1c			Pebbly sandstones interbedded with silty claystone	Decimeter-scale beds of moderately sorted, medium- to coarse-grained structureless sandstone. Sub-rounded to rounded mudstone clasts are found. Sandstone bed atop dark-grey silty claystone units has an erosive base.	
	Middle	Channel	II-2a			Pebbly to massive sandstone	Amalgamated decimeter-scale beds of pebbly, moderately to locally well sorted, quartz-rich, coarse-grained sandstones with common granules and pebbles of quartz and mudstone clasts. Occasional shell and belemnite fragments are found.	
		Lobe	II-2b			Normal-graded medium-coarse sandstone	Amalgamated decimeter-scale beds of variably (poorly to well) sorted, quartz-rich, coarse-grained sandstones with overall fining upwards. Quartz pebbles and granules concentrate in basal lags. The lower part of beds is structureless but locally display grain-size stratification.	
		Fringe	II-2c			Normal-graded medium to coarse sandstones with thin-laminated	Amalgamated decimeter-scale beds of moderately to well sorted, quartz-rich, medium-grained sandstones with overall fining upwards and coarse-grained sandstones in basal lags. Beds are structureless at the base, where occasional dewatering structures are displayed. Planar-stratification highlighted by organic-rich laminar is present at the top.	
						claystone layers		

(continued on next page)

Table 1 (continued)

Outer	Channel	II-3a			3178.5 m 3179.0 m	Normal-graded medium grained sandstone with tractional carpets	Centimeter- to decimeter-scale beds of moderately to well sorted, fine-grained sandstones intercalated with dark-grey, laminated siltstone layers. Sandstone beds fine upwards and are structureless to locally wispy banded with frequent tiny claystone clasts. Tractional lags are present at the sandy base. Rare sporadic and sparse bioturbation with <i>Chondrites</i> and <i>Phycosiphon</i> .	
	Lobe	II-3b			3082.4 m 3082.7 m	Normal-graded medium-fine sandstones interbedded with thin claystone layers	Dark-grey planar laminated siltstone and claystone with well sorted, very-fine-grained, quartz-rich sandstone. Siltstone and claystone display frequent sandy pinstripes. No erosion or tractional lags are observed at the base of sandstone beds.	
	Fringe	II-3c			3124.1m 3124.5 m	Claystone interbedded with thin layers of normal-graded medium-fine sandstone	Planar laminated siltstone and claystone dominated. Frequent light grey, very fine grained, millimeter- to centimeter-scale sandstone pinstripes throughout, which occasionally display ripple-scale cross-lamination.	
Basin plain		III			2041.3 m 2041.6 m	Dark grey offshore claystone	Dark grey silty claystone heavily bioturbated by <i>Chondrites</i> and <i>Phycosiphon</i> . Occasional belemnites are found. Millimeter- to centimeter-scale beds are separated by re-crystallized calcite laminations.	Basinal marine deposits

## Acknowledgement

We would like to thank Spirit Energy (originally Bayerngas Norge AS) for financially supporting this research and the permission to present the datasets. We thank Marianne Bruvoll and Morten Bergan for constructive discussions during the project. Our colleagues, especially Dr. Dora Luz Marin Restrepo, from the Department of Energy Resources are thanked for their valuable comments. Reviewers Dr. George Pantopoulos and Dr. David W. Jones are thanked for their constructive suggestions on improving the quality of this manuscript.

## Appendix A. Supplementary data

Supplementary data to this article can be found online at <https://doi.org/10.1016/j.marpetgeo.2020.104361>.

## References

- Allerton, S., Giuliani, E., Kwiatkowski, A., Jones, M., Robinson, J., Styles, A., 2018. Structural evolution of the T-block Brae fields, South Viking graben. In: Turner, C.C., Cronin, B.T. (Eds.), *Rift-Related Coarse-Grained Submarine Fan Reservoirs; the Brae Play, South Viking Graben, North Sea*. AAPG Memoir 115, pp. 543–563.
- Baniak, G.M., Gingras, M.K., Burns, B.A., George Pemberton, S., 2014. An example of a highly bioturbated, storm-influenced shoreface deposit: upper Jurassic Ula Formation, Norwegian North Sea. *Sedimentology* 61, 1261–1285.
- Bartholomew, I.D., Peters, J.M., Powell, C.M., 1993. Regional structural evolution of the North Sea: oblique slip and the reactivation of basement lineaments. In: *Petroleum Geology Conference Series*, pp. 1109.
- Bell, D., Kane, I.A., Pontén, A.S.M., Flint, S.S., Hodgson, D.M., Barrett, B.J., 2018. Spatial variability in depositional reservoir quality of deep-water channel-fill and lobe deposits. *Mar. Petrol. Geol.* 98, 97–115.
- Bouma, A.H., 1962. *Sedimentology of Some Flysch Deposits: a Graphic Approach to Facies Interpretation*. Elsevier, Amsterdam, pp. 168.
- Bromley, R.G., Ekdale, A.A., 1984. *Chondrites: a trace fossil indicator of anoxia in sediments*. *Science* 224, 872–874.
- Cantero, M.I., Cantelli, A., Pirmez, C., Balachandar, S., Mohrig, D., Hickson, T.A., Yeh, T.-h., Naruse, H., Parker, G., 2012. Emplacement of massive turbidites linked to extinction of turbulence in turbidity currents. *Nat. Geosci.* 5, 42.
- Corti, G., 2008. Control of rift obliquity on the evolution and segmentation of the main Ethiopian rift. *Nat. Geosci.* 1, 258.
- Cowie, P.A., Gupta, S., Dawers, N.H., 2000. Implications of fault array evolution for synrift depocentre development: insights from a numerical fault growth model. *Basin Res.* 12, 241–261.
- Crans, W., Mandl, G., Haremboure, J., 1980. On the theory of growth faulting: a geo-mechanical delta model based on gravity sliding. *J. Petrol. Geol.* 2, 265–307.
- Ebinger, C., 2005. Continental break-up: the east african perspective. *Astron. Geophys.* 46, 2.16–2.21.
- Ebinger, C., Jackson, J., Foster, A., Hayward, N., 1999. Extensional basin geometry and the elastic lithosphere. *Phil. Trans. Roy. Soc. Lond.: Math. Phys. Eng. Sci.* 357, 741–765.
- Færseth, R.B., Knudsen, B.-E., Liljedahl, T., Midbøe, P., Söderstrøm, B., 1997. Oblique rifting and sequential faulting in the Jurassic development of the northern North Sea. *J. Struct. Geol.* 19, 1285–1302.
- Fazlikhani, H., Fossen, H., Gawthorpe, R.L., Faleide, J.I., Bell, R.E., 2017. Basement structure and its influence on the structural configuration of the northern North Sea rift. *Tectonics* 36, 1151–1177.
- Fossen, H., Khani, H.F., Faleide, J.I., Ksienzyk, A.K., Dunlap, W.J., 2017. Post-Caledonian extension in the West Norway–northern North Sea region: the role of structural inheritance. *Geol. Soc. Lond. Special Publ.* 439, 465–486.
- Fossen, H., Schultz, R.A., Rundhovde, E., Rotevatn, A., Buckley, S.J., 2010. Fault linkage and graben stepovers in the Canyonlands (Utah) and the North Sea Viking Graben, with implications for hydrocarbon migration and accumulation. *AAPG (Am. Assoc. Pet. Geol.) Bull.* 94, 597–613.
- Galloway, W.E., 1998. Siliciclastic Slope and base-of-slope depositional systems: component facies, stratigraphic architecture, and classification. *AAPG (Am. Assoc. Pet. Geol.) Bull.* 82, 569–595.
- Gawthorpe, R., Hurst, J., 1993. Transfer zones in extensional basins: their structural style and influence on drainage development and stratigraphy. *J. Geol. Soc.* 150, 1137–1152.
- Gawthorpe, R.L., Leeder, M.R., 2000. Tectono-sedimentary evolution of active extensional basins. *Basin Res.* 12, 195–218.
- Ghibaudo, G., 1992. Subaqueous sediment gravity flow deposits: practical criteria for their field description and classification. *Sedimentology* 39, 423–454.
- Gormly, J.R., Buck, S.P., Chung, H.M., 1994. Oil-source rock correlation in The north viking graben. *Org. Geochem.* 22, 403–413.

- Hampson, G.J., Storms, J.E., 2003. Geomorphological and sequence stratigraphic variability in wave-dominated, shoreface-shelf parasequences. *Sedimentology* 50, 667–701.
- Hayward, N.J., Ebinger, C.J., 1996. Variations in the along-axis segmentation of the Afar Rift system. *Tectonics* 15, 244–257.
- Herbosch, A., Verniers, J., 2014. Stratigraphy of the lower palaeozoic of the brabant massif, Belgium, part II: the middle Ordovician to lowest silurian of the Rebecq Group. *Geol. Belg.* 17, 115–136.
- Hodgson, D.M., 2009. Distribution and origin of hybrid beds in sand-rich submarine fans of the Tanqua depocentre, Karoo Basin, South Africa. *Mar. Petrol. Geol.* 26, 1940–1956.
- Hofstra, M., Pontén, A.S.M., Peakall, J., Flint, S.S., Nair, K.N., Hodgson, D.M., 2017. The impact of fine-scale reservoir geometries on streamline flow patterns in submarine lobe deposits using outcrop analogues from the Karoo Basin. *Petrol. Geosci.* 23, 159–176.
- Hospers, J., Ediriweera, K.K., 1991. Depth and configuration of the crystalline basement in the viking graben area, northern North sea. *J. Geol. Soc.* 148, 261–265.
- Hoth, S., Knaust, D., Sánchez-López, A., Kassold, S., Sviland-Østre, S., 2018. The Gudrun field: gravity-flow deposition during rifting and inversion. In: Turner, C.C., Cronin, B.T. (Eds.), *Rift-Related Coarse-Grained Submarine Fan Reservoirs; the Brae Play, South Viking Graben, North Sea*. AAPG Memoir 115, pp. 387–421.
- Jackson, C.A.L., Larsen, E., Hanslien, S., Tjemsland, A.E., 2011. Controls on synrift turbidite deposition on the hanging wall of the South Viking Graben, North Sea rift system, offshore Norway. *AAPG (Am. Assoc. Pet. Geol.) Bull.* 95, 1557–1587.
- Jacquin, T., Dardeau, G., Durllet, C., de Graciansky, P.-C., Hantzpergue, P., 1998. The North Sea cycle: an overview of 2nd-order transgressive/regressive facies cycles in western Europe. In: De Graciansky, P.-C., Hardenbol, J., Jacquin, T., Vail, P.R. (Eds.), *Mesozoic and Cenozoic Sequence Stratigraphy of European Basins*. SEPM Special Publication, Tulsa, pp. 445–466.
- Kernen, R.A., Giles, K.A., Rowan, M.G., Lawton, T.F., Hearon, T.E., 2012. Depositional and halokinetic-sequence stratigraphy of the Neoproterozoic Wonoka formation adjacent to patawarta allochthonous salt sheet, central flinders ranges, south Australia. *Geol. Soc. Lond. Special Publ.* 363, 81–105.
- Khalil, S., McClay, K., 2001. Tectonic evolution of the NW red sea-Gulf of sues rift system. *Geol. Soc. Lond. Special Publ.* 187, 453–473.
- Kneller, B.C., Branney, M.J., 1995. Sustained high-density turbidity currents and the deposition of thick massive sands. *Sedimentology* 42, 607–616.
- Leclair, S.F., Arnott, R.W.C., 2005. Parallel lamination formed by high-density turbidity currents. *J. Sediment. Res.* 75, 1–5.
- Leeder, M.R., 1993. Tectonic controls upon drainage basin development, river channel migration and alluvial architecture: implications for hydrocarbon reservoir development and characterization. *Geol. Soc. Lond. Special Publ.* 73, 7–22.
- Marr, J.G., Shanmugam, G., Parker, G., 2001. Experiments on subaqueous sandy gravity flows: the role of clay and water content in flow dynamics and depositional structures. *Bull. Geol. Soc. Am.* 113, 1377–1386.
- McArthur, A.D., Hartley, A.J., Archer, S.G., Jolley, D.W., Lawrence, H.M., 2016. Spatiotemporal relationships of deep-marine, axial and transverse depositional systems from the synrift Upper Jurassic of the Central North Sea. *AAPG (Am. Assoc. Pet. Geol.) Bull.* 100, 1469–1500.
- McClay, K.R., Dooley, T., Whitehouse, P., Mills, M., 2002. 4-D evolution of rift systems: insights from scaled physical models. *AAPG (Am. Assoc. Pet. Geol.) Bull.* 86, 935–959.
- Mckee, E.D., Weir, G.W., 1953. Terminology for stratification and cross-stratification in sedimentary rocks. *GSA Bull.* 64, 381–390.
- Middleton, G.V., Hampton, M.A., 1973. Sediment gravity flows: mechanics of flow and deposition. In: Middleton, G.V., Bouma, A.H. (Eds.), *Turbidity and Deep Water Sedimentation*. Society for Sedimentary Geology, pp. 1–38.
- Mulder, T., Alexander, J., 2001. The physical character of subaqueous sedimentary density flows and their deposits. *Sedimentology* 48, 269–299.
- Mulder, T., Migeon, S., Savoye, B., Faugères, J.-C., 2001. Inversely graded turbidite sequences in the deep Mediterranean: a record of deposits from flood-generated turbidity currents? *Geo Mar. Lett.* 21, 86–93.
- Nemec, W., Steel, R.J., 1984. Alluvial and coastal conglomerates: their significant features and some comments on gravelly mass-flow deposits. In: Koster, E.H., Steel, R.J. (Eds.), *Sedimentology of Gravels and Conglomerates*. Canadian Society of Petroleum Geologists, pp. 1–31.
- Nottvedt, A., Gabrielsen, R.H., Steel, R.J., 1995. Tectonostratigraphy and sedimentary architecture of rift basins, with reference to the northern North Sea. *Mar. Petrol. Geol.* 12, 881–901.
- NPD, 2019. FactMaps of the Norwegian Petroleum Directorate. [http://gis.npd.no/factmaps/html\\_21/](http://gis.npd.no/factmaps/html_21/), Accessed date: 20 January 2019.
- Odinsen, T., Christiansson, P., Gabrielsen, R.H., Faleide, J.I., Berge, A.M., 2000a. The geometries and deep structure of the northern North Sea rift system. *Geol. Soc. Lond. Special Publ.* 167, 41–57.
- Odinsen, T., Reemst, P., Van Der Beek, P., Faleide, J.I., Gabrielsen, R.H., 2000b. Permo-Triassic and Jurassic extension in the northern North Sea: results from tectonostratigraphic forward modelling. *Geol. Soc. Lond. Special Publ.* 167, 83–103.
- Peacock, D.C.P., Sanderson, D.J., 1994. Geometry and development of relay ramps in normal fault systems. *AAPG (Am. Assoc. Pet. Geol.) Bull.* 78, 147–165.
- Picot, M., Droz, L., Marsset, T., Dennielou, B., Bez, M., 2016. Controls on turbidite sedimentation: insights from a quantitative approach of submarine channel and lobe architecture (Late Quaternary Congo Fan). *Mar. Petrol. Geol.* 72, 423–446.
- Piper, D.J.W., Normark, W.R., 1983. Turbidite depositional patterns and flow characteristics, Navy submarine fan, California borderland. *Sedimentology* 30, 681–694.
- Postma, G., 1986. Classification for sediment gravity-flow deposits based on flow conditions during sedimentation. *Geology* 14, 291–294.
- Postma, G., Cartigny, M.J.B., 2014. Supercritical and subcritical turbidity currents and their deposits - a synthesis. *Geology* 42, 987–990.
- Poulimenos, G., Zelliidis, A., Kontopoulos, N., Doutsos, T., 1993. Geometry of trapezoidal fan deltas and their relationship to extensional faulting along the southwestern active margins of the Corinth rift, Greece. *Basin Res.* 5, 179–192.
- Prosser, S., 1993. Rift-related linked depositional systems and their seismic expression. *Geol. Soc. Lond. Special Publ.* 71, 35–66.
- Raiswell, R., Berner, R.A., 1985. Pyrite formation in euxinic and semi-euxinic sediments. *Am. J. Sci.* 285, 710–724.
- Ravnås, R., Bondevik, K., 1997. Architecture and controls on Bathonian-Kimmeridgian shallow-marine synrift wedges of the Oseberg-Brage area, northern North Sea. *Basin Res.* 9, 197–226.
- Ravnås, R., Nøttvedt, A., Steel, R., Windelstad, J., 2000. syn-rift sedimentary architectures in the northern North sea. *Geol. Soc. Lond. Special Publ.* 167, 133–177.
- Ravnås, R., Steel, R.J., 1998. Architecture of marine rift-basin successions. *AAPG (Am. Assoc. Pet. Geol.) Bull.* 82, 110–146.
- Ravnås, R., Windelstad, J., Mellere, D., Nøttvedt, A., Sjøblom, T.S., Steel, R.J., Wilson, R.C.L., 1997. A marine Late Jurassic syn-rift succession in the Lusitanian Basin, western Portugal - tectonic significance of stratigraphic signature. *Sediment. Geol.* 114, 237–266.
- Rowland, J., Sibson, R., 2001. Extensional fault kinematics within the Taupo Volcanic Zone, New Zealand: soft-linked segmentation of a continental rift system. *N. Z. J. Geol. Geophys.* 44, 271–283.
- Rowland, J., Sibson, R., 2004. Structural controls on hydrothermal flow in a segmented rift system, Taupo Volcanic Zone, New Zealand. *Geofluids* 4, 259–283.
- Scott, A.S.J., Ottesen, S., 2018. Tectono-stratigraphic development of the upper Jurassic in the Johan Sverdrup area (Extended abstract). In: Turner, C.C., Cronin, B.T. (Eds.), *Rift-Related Coarse-Grained Submarine Fan Reservoirs; the Brae Play, South Viking Graben, North Sea*. AAPG Memoir 115, pp. 445–451.
- Shanmugam, G., Moiola, R.J., 1991. Types of submarine fan lobes: models and implications. *AAPG (Am. Assoc. Pet. Geol.) Bull.* 75, 156–179.
- Sleep, N.H., Blanpied, M.L., 1992. Creep, compaction and the weak rheology of major faults. *Nature* 359, 687–692.
- Spychala, Y.T., Hodgson, D.M., Lee, D.R., 2017. Autogenic controls on hybrid bed distribution in submarine lobe complexes. *Mar. Petrol. Geol.* 88, 1078–1093.
- Stewart, D.J., Schwander, M., Bolle, L., 1995. Jurassic depositional systems of the horda platform, Norwegian north sea: practical consequences of applying sequence stratigraphic models. In: Steel, R.J., Felt, V.L., Johannessen, E.P., Mathieu, C. (Eds.), *Norwegian Petroleum Society Special Publications*. Elsevier, pp. 291–323.
- Stow, D.A.V., Huc, A.Y., Bertrand, P., 2001. Depositional processes of black shales in deep water. *Mar. Petrol. Geol.* 18, 491–498.
- Stow, D.A.V., Johansson, M., 2000. Deep-water massive sands: nature, origin and hydrocarbon implications. *Mar. Petrol. Geol.* 17, 145–174.
- Talling, P.J., Masson, D.G., Sumner, E.J., Malgesini, G., 2012. Subaqueous sediment density flows: depositional processes and deposit types. *Sedimentology* 59, 1937–2003.
- Upcott, N.M., Mukasa, R.K., Ebinger, C.J., Karner, G.D., 1996. Along-axis segmentation and isostasy in the Western rift, East Africa. *J. Geophys. Res.: Solid Earth* 101, 3247–3268.
- Vollset, J., Doré, A.G., 1984. A Revised Triassic and Jurassic Lithostratigraphic Nomenclature for the Norwegian North Sea. Norwegian Petroleum Directorate, Stavanger, pp. 1–53.
- Wells, M.J., 1999. Coarse-grained, deep-water sedimentation along a border fault margin of Lake Malawi, Africa: seismic stratigraphic analysis. *J. Sediment. Res.* 69, 832–846.
- Wentworth, C.K., 1922. A scale of Grade and class terms for clastic sediments. *J. Geol.* 30, 377–392.
- Whipp, P.S., Jackson, C.A.L., Gawthorpe, R.L., Dreyer, T., Quinn, D., 2014. Normal fault array evolution above a reactivated rift fabric; a subsurface example from the northern Horda Platform, Norwegian North Sea. *Basin Res.* 26, 523–549.
- Wolfenden, E., Ebinger, C., Yirgu, G., Deino, A., Ayalew, D., 2004. Evolution of the northern Main Ethiopian rift: birth of a triple junction. *Earth Planet. Sci. Lett.* 224, 213–228.
- Wright, T.J., Ebinger, C., Biggs, J., Ayele, A., Yirgu, G., Keir, D., Stork, A., 2006. Magma-maintained rift segmentation at continental rupture in the 2005 Afar dyking episode. *Nature* 442, 291.
- Zeiss, A., 2003. The upper Jurassic of Europe: its subdivision and correlation. *Geol. Surv. Den. Greenl. Bull.* 1, 75–114.
- Zhong, X., Escalona, A. (in press) Evidences of rift segmentation and controls of middle to late Jurassic syn-rift deposition in the Ryggsteinen Ridge area, northern North sea. *AAPG (Am. Assoc. Pet. Geol.) Bull.* <http://dx.doi.org/10.1306/03172018173>.
- Zhong, X., Escalona, A., Sverdrup, E., Bukta, K., 2018. Impact of fault evolution in Gilbert-type fan deltas in the Evrostini area, south-central Gulf of Corinth, Greece. *Mar. Petrol. Geol.* 95, 82–99.
- Ziegler, P., 1975. Geologic evolution of North Sea and its tectonic framework. *AAPG (Am. Assoc. Pet. Geol.) Bull.* 59, 1073–1097.